Design and Implementation of Linearized CMOS Mixer for RF Application

AU-YEUNG Chung-Fai

A Thesis Submitted in Partial Fulfillment

of the Requirements for the Degree of

Master of Philosophy

in

Electronic Engineering

June 2003

ABSTRACT

Linearity is an essential requirement in modern wireless communication systems due to the small channel spacing. Various linearization schemes have been studied extensively for power amplifiers, but much less attention has been paid to mixers. In this thesis, the application of generalized low-frequency signal injection technique to the linearization of doubly balanced dual-gate mixer is presented. The reason that the proposed injection method shows better linearity performance than the conventional case is analytically derived. Issues related to optimum operating conditions and bandwidth limitation are examined. For experimental verification, a down-conversion mixer is designed and fabricated using AMS 0.35 μm CMOS technology. It operates at an RF input frequency of 900 MHz, a voltage supply of 2 V, a LO power of –7 dBm and a total current consumption of 3.6 mA. For the linearization scheme, a third-order IMD reduction factor of more than 30 dB is observed over a wide dynamic range.

摘要

在頻道濟迫的無綫通信系統中，原件的綫性特性是一個非常重要的一環。目前各種綫性化技術的研究主要針對的是在功率放大器上的應用，而涉及混頻器方面的研究則不多。本論文說明如何應用一種全新的低頻信號注射技術來實現雙平衡雙門混頻器綫性化的原理。論文以數學解述這種技術爲何較傳統方法在綫性性能上優勝，並推導出最佳工作條件和帶寬限制。在實驗方面，此研究採用了 AMS 0.35 μm CMOS 技術設計製造了一個下變頻混頻器。該混頻器的射頻輸入頻率是 900MHz，電源供電是 2V，本振功率爲 －7 dBm，而總工作電流爲 3.6 mA。在綫性性能方面，該器件在一個很寬的動態範圍內實現了高於 30 dB 的三階雙音互調失真優化因子。

ACKNOWLEDGEMENTS

I would like to thank to my supervisor, Prof. K.K.M. Cheng, for his skilful scientific guidance, innovative ideas and encouragement throughout this research project.

I would like to express my gratitude to my colleagues, S. H. Cheng, K. P. Chan, T. C. Leung and F. L. Wong. Thanks for their suggestions and advice in my research.

Finally, I would like to thank to my family for their patience and support in this two years.

CONTENTS

CHAPTER 1

INTRODUCTION

MOSFET (metal-oxide-semiconductor field-effect transistor) was fabricated for the first time in the sixties. It is the basic building block of very large-scale integrated (VLSI) circuits. In the past decades, CMOS technology has led to the rapid development of digital systems including computers and communication applications. CMOS technology has also become increasingly popular for RF integrated circuit (RFIC) design.

The primary purpose of a mixer is to translate a signal from one frequency to another. Since amplifiers, filters, and detectors are more cost-effective to be operated at lower frequencies, therefore mixer is a very popular building block in most transceiver modules. Nowadays, RF mixers are often realized in monolithic form which offers advantages such as small size, low-cost in large-volume production. In the early days of integrated circuit technology, it was known that FET mixer offers advantages like conversion gain and compatibility with monolithic processing. Conversion gain improves the system noise figure, reduces the number of amplification stages and improves the dynamic range of the receiver.

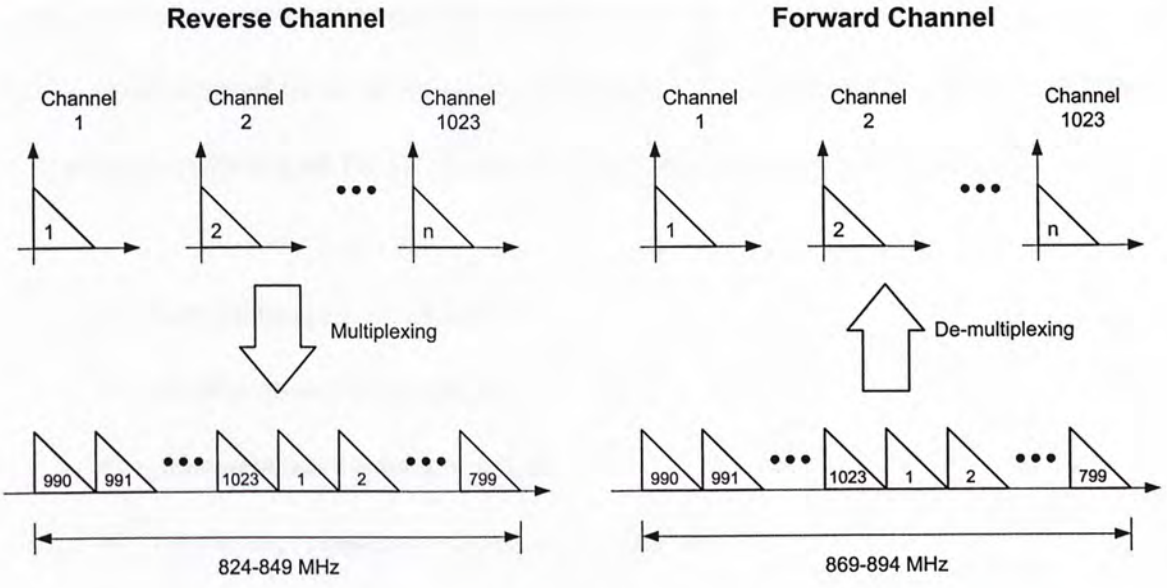

	Channel Number	Center Frequency (MHz)
Reverse Channel	$1 \le N \le 799$	$0.03N + 825$
	$990 \le N \le 1023$	$0.03(N - 1023) + 825$
Forward Channel	$1 \le N \le 799$	$0.03N + 870$
	$990 \le N \le 1023$	$0.03(N - 1023) + 870$

(Channels 800-989 are unused)

Figure 1.1 Frequency spectrum allocation for the U.S. cellular radio service

Figure 1.1 illustrates the frequency spectrum allocation for U.S. cellular radio service. Frequency division multiple access (FDMA) is used in this system. Communication channels are frequency multiplexed together to maximize transmission capacity. Frequency multiplexing and de-multiplexing rely heavily on the use of mixers and channel selection filters.

Figure 1.2 shows the block diagram of a simplified integrated transceiver unit. In the transmitter side, a mixer is used to up-convert the IF signal to RF frequency for

subsequent transmission through the antenna. In the receiver side, RF signal is amplified and down-converted to the IF frequency for further channel filtering and demodulation. The general requirements for the design of mixer can be summarized as follows:

- Conversion gain (if possible)
- Good port-to-port isolation
- Low spurious signal generation
- Low power consumption and LO requirement
- Low noise figure
- High linearity

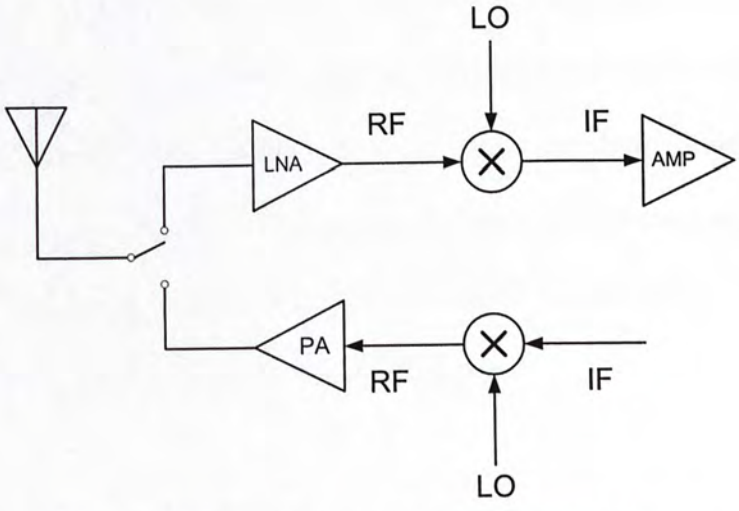

Figure 1.2 Simplified integrated transceiver block diagram

In the presence of device nonlinearities, the output signal of mixer is usually distorted. As illustrated in Figure 1.3, the output spectrum has spill-over of energy from the main channel to the adjacent channels, due to the generation of intermodulation distortion (Spectral Regrowth). In FDMA system, spectral regrowth causes problems like

cross talk, and undesired interference to other users. Fortunately, linearization method may be applied to minimize such nonlinear distortion.

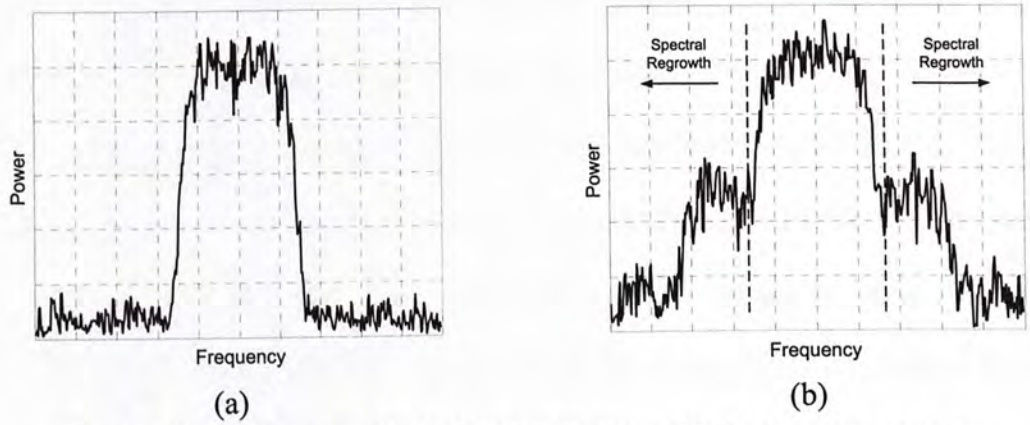

Figure 1.3 Spectral regrowth (a) CDMA input spectrum (b) CDMA output spectrum

Linearity is an essential requirement in modern communication systems due to the small channel spacing. The dynamic range of a RF transceiver is often limited by the linearity of mixers and amplifiers (LNA) in the receiving chain. Various linearization schemes have been studied extensively for power amplifiers, however much less attention has been paid to mixer design. Linearization approaches for mixers such as feed-forward, predistortion and feedback have been reported recently.

The main objective of this thesis is to investigate new linearization method in applying to CMOS doubly balanced dual-gate mixer. Generalized "Low frequency signal injection method" is proposed for the suppression of the third-order intermodulation products. The organization of this thesis is summarized as follows:

Chapter 2 describes basic theory and the electrical properties of mixers. Various architectures of mixer are reviewed. Chapter 3 presents the design and implementation of

doubly balanced dual-gate mixer based on CMOS technology. Moreover, layout consideration on CMOS mixer design is discussed. Then, a review of linearization schemes for mixer is given in Chapter 4. Chapter 5 introduces the generalized low-frequency signal injection method for mixer linearization. Practical issues related to gain and phase mismatches are also addressed. For experimental verification, measured performances of a CMOS down-conversion mixer are given in Chapter 6. Both single and dual signal injection schemes of the linearization method are tested using two-tone and vector-modulated signal formats. Finally, conclusions and recommendations for future work are provided in chapter 7.

CHAPTER 2

BASIC THEORY OF MIXER

A mixer is fundamentally a multiplier [1]. The ideal mixing response can be represented by trigonometric identity:

$$V_{out}(t) = A\cos(\omega_{RF}t)\cdot B\cos(\omega_{LO}t)$$

$$= \frac{AB}{2}\left[\cos(\omega_{RF}+\omega_{LO})t + \cos(\omega_{RF}-\omega_{LO})t\right] \qquad (2.1)$$

Equation (2.1) shows that if a signal of frequency ω_{RF} is mixed with another signal of frequency ω_{LO}, the output will consist of two signals of frequencies equal to $\omega_{RF}+\omega_{LO}$ and $\omega_{RF}-\omega_{LO}$.

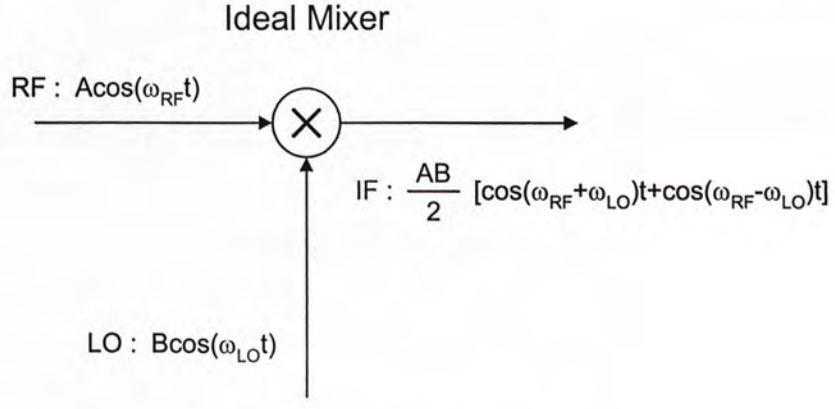

Figure 2.1 Ideal mixing response

Unfortunately, no device can perform perfect multiplication. The non-ideal input-output characteristics of a mixer can be described by a power series (2.2).

$$V_{out}(t) = V_{LO}(t)\left[a_0 + a_1V_{RF}(t) + a_2V_{RF}(t)^2 + a_3V_{RF}(t)^3 + \ldots\right] \qquad (2.2)$$

Further mathematical manipulation shows that the nonlinear device may generate many harmonics and mixing products other than the desired one. Consider down-converted operation, in the presence of two-tone RF signals, the down-converted output will consist of the main-tone inputs as well as intermodulation distortion (IMD) components, as illustrated in Figure 2.2. Linearity performance of a mixer is usually characterized by using 1-dB compression point, 2nd order intercept point, 3rd order intercept point, blocking dynamic range and spurious free dynamic range [2-3]. The higher the values of these parameters imply that the device exhibit higher linearity.

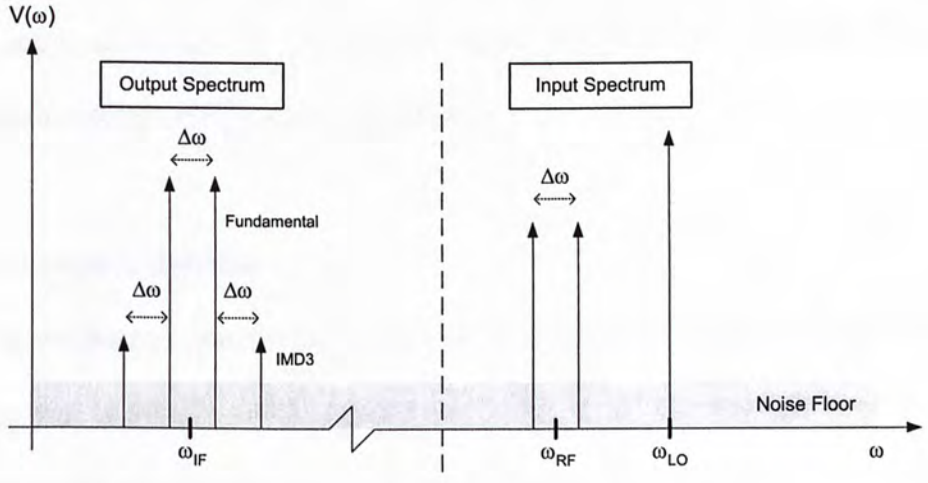

Figure 2.2 Mixer input/output spectrum

2.1 DEFINITION OF MIXER'S ELECTRICAL PARAMETERS

2.1.1 Conversion gain

Conversion gain can be quoted as voltage or power gain. When both input and output of the device are properly matched, the voltage gain will be equal to power gain. Power conversion gain is defined as the ratio of the desired IF output power to the RF input power. For the mixer described by equation (2.1), the conversion gain G_c is B/2.

Passive mixer generally has power lost during frequency conversion. The conversion gain of active mixer can be greater than unity. Therefore, active mixer often provides amplification along with frequency translation.

2.1.2 Port-to-port isolation

It is desirable to minimize interaction between the RF, LO and IF ports. For instance, the LO power is usually much higher than the RF signal and any LO feedthrough to the IF output might cause problem in subsequent stages. This problem is exacerbated if the IF and LO have similar frequency where filtering is ineffective and IF signal is heavily distorted. For a good mixer design, RF and LO signals should not be presented at the IF output.

LO to RF isolation is important too. Poor reverse isolation permits the strong LO signal, or even its harmonics, to be radiated at RF receiving antenna and may cause

interference to other receivers. Thus, port-to-port isolation should be kept as high as possible.

2.1.3 Noise Figure

Mixer's noise figure is defined as the signal-to-noise ratio at the RF input port divided by the signal-to-noise ratio at the IF output port. It is described by equation (2.3).

$$NF = \frac{S/N|_{RF}}{S/N|_{IF}}$$

$$= \frac{N|_{IF}}{G_c N|_{RF}} \tag{2.3}$$

Typically, there are two input frequency that will generate the same IF frequency. One is the desired RF signal and the other is called image signal. As illustrated by Figure 2.3, the signal frequency below ω_{LO} is known as "Lower Sideband", where as the signal frequency above ω_{LO} is termed the "Upper Sideband". The frequency spacing between the RF and image signal is $2\omega_{IF}$.

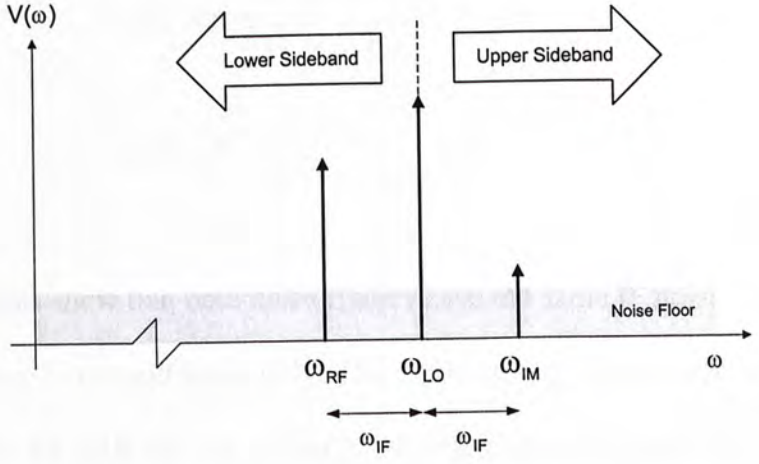

Figure 2.3 Mixer signal sidebands

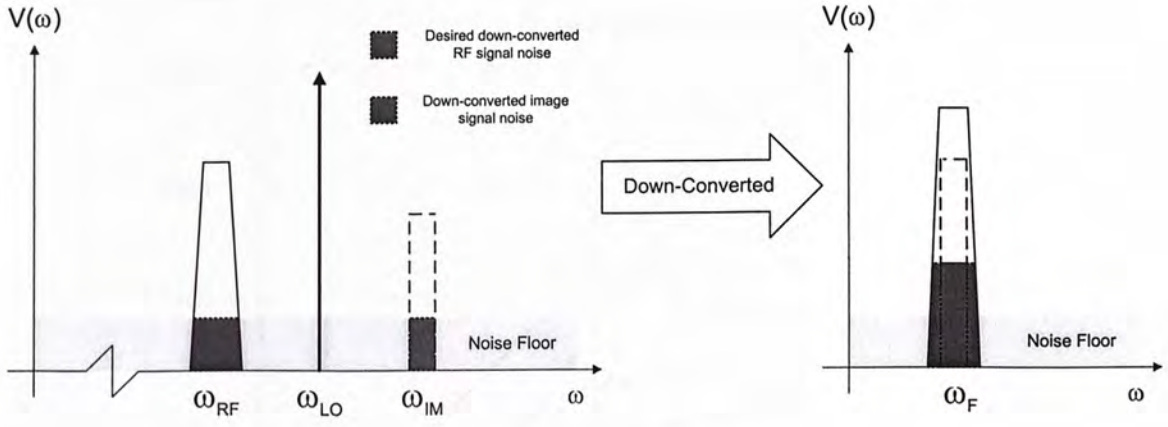

Figure 2.4 Down-converted noise power

Consider the down-converted operation (Figure 2.4), both the RF signal noise and image signal noise may be transformed to the IF noise. The presence of the image signal complicates the noise figure computations. In the case there exists RF signal (Lower Sideband) only, the noise figure thus measured is called single-sideband noise figure (SSB NF). On the contrary, if both the RF and image signals exist, the measured noise figure is called double-sideband noise figure (DSB NF). The computations of SSB NF and DSB NF are given by equation (2.4) and (2.5).

$$SSB\ NF = \frac{N|_{IF}}{G_c N_{SSB}|_{RF}} \tag{2.4}$$

$$DSB\ NF = \frac{N|_{IF}}{G_c N_{DSB}|_{RF}} \tag{2.5}$$

These equations show that both noise figures have the same IF noise, but SSB NF has signal noise power in one sideband only. The input noise power is theoretically half the value of DSB NF. So, SSB NF will normally be 3 dB higher than DSB NF.

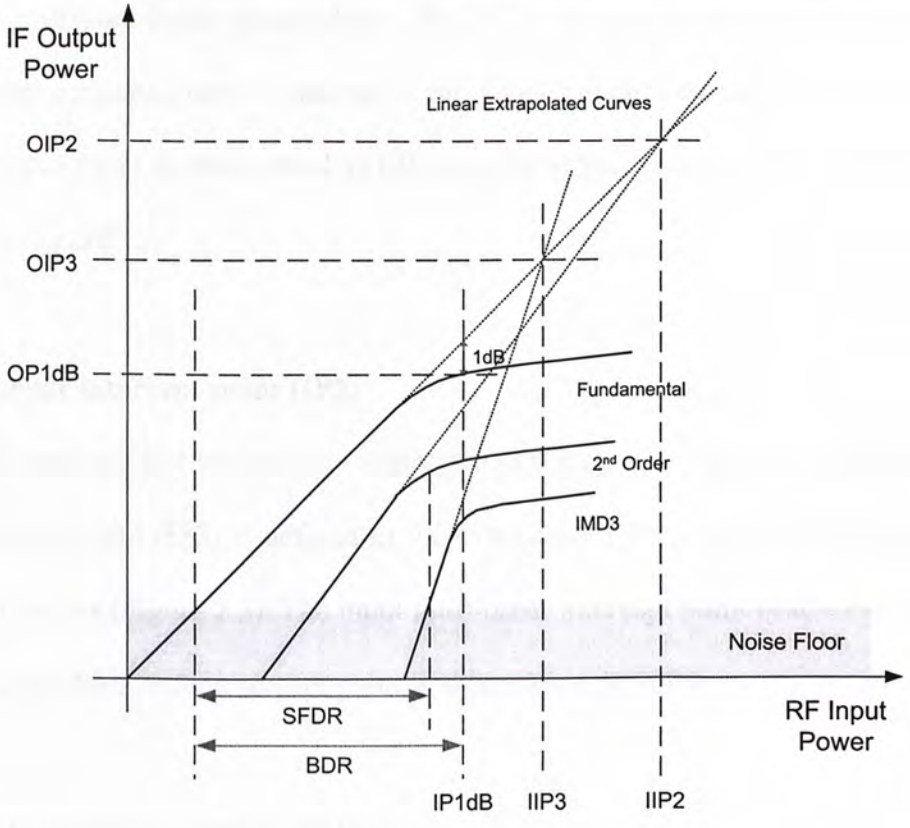

Figure 2.5 Mixer linearity parameters

2.1.4 1-dB compression point (P1dB)

As illustrated in Figure 2.5, the output fundamental is compressed at certain input power level. The effect is described by 1-dB compression point (P1dB). It is defined as the signal level that causes the conversion gain to drop by 1 dB. The value of compression point is usually quoted depending on whether it is input- or output-referred. The input P1dB is abbreviated as IP1dB and the output P1dB is abbreviated as OP1dB.

2.1.5 2nd order intercept point (IP2)

When specifying the mixer's 2nd order intercept point (IP2), it is assumed that only the fundamental RF and LO frequencies are applied to the mixer ports and that the harmonic

distortion is created in the mixer alone. The IP2 is derived by extrapolating the mixer's second-order response until it intercepts the fundamental response. The input second-order intercept point is abbreviated as IIP2 and the output second-order intercept point is abbreviated as OIP2.

2.1.6 3rd order intercept point (IP3)

Under two-tone test excitation, intermodulation distortion will be generated. The 3rd order intercept point (IP3) is defined as the extrapolated intersection of the fundamental and IMD3 curves (Figure 2.5). The input third-order intercept point is abbreviated as IIP3 and the output third-order intercept point is abbreviated as OIP3.

2.1.7 Blocking dynamic range (BDR)

The blocking dynamic range (BDR) is defined as the ratio of 1-dB compression point to noise floor. It measures a device's ability of strong signal toleration that without desensitizing the device.

2.1.8 Spurious free dynamic range (SFDR)

The spurious free dynamic range (SFDR) is defined as the signal-to-noise ratio corresponding to the input amplitude at which an undesired intermodulation product just equals the noise power. It measures the input power range which makes the output is free of spurs when two-tone signals are applied to the device.

2.2 REVIEW OF MIXER ARCHITECTURES

The different architectures of mixer provide different operation properties [1]. Passive mixer offers excellent third-order intercept points but poor conversion gain and noise figure. It always requires a higher LO power level. Active mixers can be implemented by bipolar or FET device [4-24]. They have advantages such as conversion gain and compatible to monolithic integration. The use of active mixer lowers the overall noise figure and reduces the number of amplification stages required in a system. Various active mixer designs have been studied and implemented in different technologies. These architectures will be reviewed in the following section.

2.2.1 Diode mixer

Diode is the most simplest mixer architecture. The mixing process of diode mixer is caused by the time-varying conductance g(t):

$$g(t) = G_o + G_1 \cos(\omega_{LO} t) \tag{2.6}$$

Equation (2.7) illustrates that when a sinusoidal signal with frequency ω_{RF} is applied to the diode mixer, the resulting current contains mixing products at $\omega = \omega_{RF} - \omega_{LO}$ and $\omega = \omega_{RF} + \omega_{LO}$.

$$\begin{aligned} i(t) &= g(t)V_s(t) \\ &= G_o V_s \cos(\omega_{RF} t) + \frac{G_1 V_s}{2}\left[\cos((\omega_{RF} - \omega_{LO})t) + \cos((\omega_{RF} + \omega_{LO})t)\right] \end{aligned} \tag{2.7}$$

Simple diode mixer exhibits moderate port-to-port isolation and conversion loss.

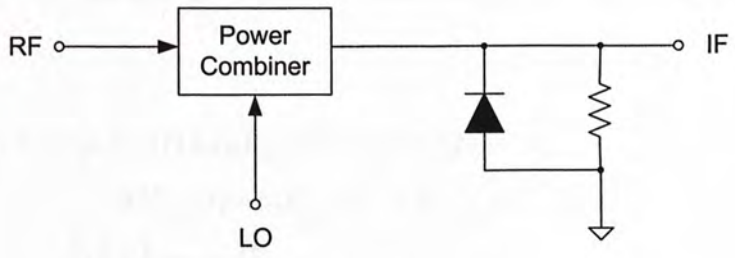

Figure 2.6 Diode mixer

2.2.2 Dual-gate mixer

Dual-gate mixer provides good LO to RF isolation. As shown in Figure 2.7, the operating principle of a dual-gate device can be illustrated by using two cascade-connected single-gate FET. In order to provide signal mixing, the lower FET is biased for RF transconductor operation. The gate bias of the upper FET is adjusted so that the device is switching on and off every half LO cycle to produce signal mixing. Finally, the IF component is extracted from the drain terminals of the dual-gate structure.

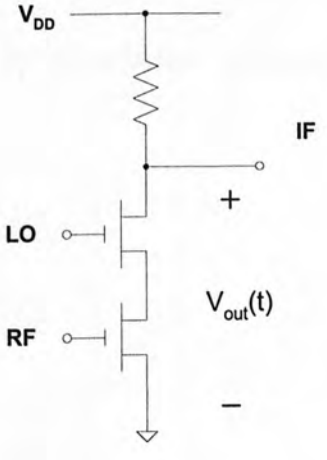

Figure 2.7 Dual-gate mixer

In practice, the non-ideal mixer's properties such as finite port-to-port isolation and

noise rejection are always presented. Mathematically, the output signal can be represented by,

$$\begin{aligned} V_{out}(t) = G_c\Big[a_1 V_{IF}(t) + a_2 V_{IF}(t)^2 + a_3 V_{IF}{}^3(t) + \cdots\Big] \\ + \frac{1}{L_1}\begin{bmatrix} b_1 V_{\omega_{RF}}(t) + b_2 V_{\omega_{RF}}(t)^2 + b_3 V_{\omega_{RF}}(t)^3 + \cdots \\ + V_{Noise,RF}(t) \end{bmatrix} \\ + \frac{1}{L_2}\begin{bmatrix} c_1 V_{\omega_{LO}}(t) + c_2 V_{\omega_{LO}}(t)^2 + c_3 V_{\omega_{LO}}(t)^3 + \cdots \\ + V_{Noise,LO}(t) \end{bmatrix} \end{aligned} \tag{2.8}$$

Where Gc is conversion gain, L_1 is RF-IF isolation and L_2 is LO-IF isolation. The functions $V_{noise,RF}(t)$ and $V_{noise,LO}(t)$ denote the noise from RF and LO port respectively.

2.2.3 Singly balanced mixer

The structure of the mixer is illustrated in Figure 2.8. Singly balanced mixer has performance advantages compared to unbalanced mixer. Singly balanced mixer requires a differential LO signal, and a pair of differential outputs. These differential configurations can be obtained by using balun. Subsequently, the output signal may be expressed as:

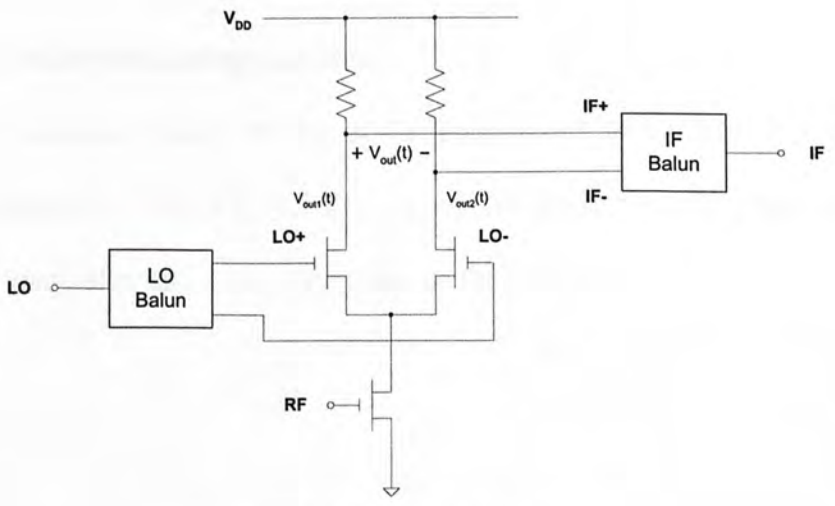

Figure 2.8 Singly balanced mixer

$$
\begin{aligned}
V_{out}(t) &= V_{out1}(t) - V_{out2}(t) \\
&= G_c\left[a_1 V_{IF}(t) + a_2 V_{IF}(t)^2 + a_3 V_{IF}{}^3(t) + \cdots\right] \\
&\quad + \frac{1}{L_1}\begin{bmatrix} b_1 V_{\omega_{RF}}(t) + b_2 V_{\omega_{RF}}(t)^2 + b_3 V_{\omega_{RF}}(t)^3 + \cdots \\ + V_{Noise,RF}(t) \end{bmatrix} \\
&\quad + \frac{1}{L_2}\begin{bmatrix} c_1 V_{\omega_{LO}}(t) + c_2 V_{\omega_{LO}}(t)^2 + c_3 V_{\omega_{LO}}(t)^3 + \cdots \\ + V_{Noise,LO}(t) \end{bmatrix} \\
&\quad - G_c\left[-a_1 V_{IF}(t) + a_2 V_{IF}(t)^2 - a_3 V_{IF}{}^3(t) + \cdots\right] \\
&\quad - \frac{1}{L_2}\begin{bmatrix} -c_1 V_{\omega_{LO}}(t) + c_2 V_{\omega_{LO}}(t)^2 - c_3 V_{\omega_{LO}}(t)^3 + \cdots \\ + V_{Noise,LO}(t) \end{bmatrix} \\
&= 2G_c\left[a_1 V_{IF}(t) + a_3 V_{IF}{}^3(t) + a_5 V_{IF}{}^5(t) + \cdots\right] \\
&\quad + \frac{1}{L_1}\begin{bmatrix} b_1 V_{\omega_{RF}}(t) + b_2 V_{\omega_{RF}}(t)^2 + b_3 V_{\omega_{RF}}(t)^3 + \cdots \\ + V_{Noise,RF}(t) \end{bmatrix} \\
&\quad + \frac{2}{L_2}\left[c_1 V_{\omega_{LO}}(t) + c_3 V_{\omega_{LO}}(t)^3 + c_5 V_{\omega_{LO}}(t)^5 + \cdots\right]
\end{aligned}
\tag{2.9}
$$

Equation (2.9) shows that the mixer can provide rejection of LO noise and even-order distortion comes from the LO.

2.2.4 Doubly balanced dual-gate mixer

A doubly balanced mixer consists of 4 simple mixers with proper interconnection as shown in Figure 2.9. Both RF and LO signals are applied to the mixer in differential mode. Mathematically, the output signal can be derived as:

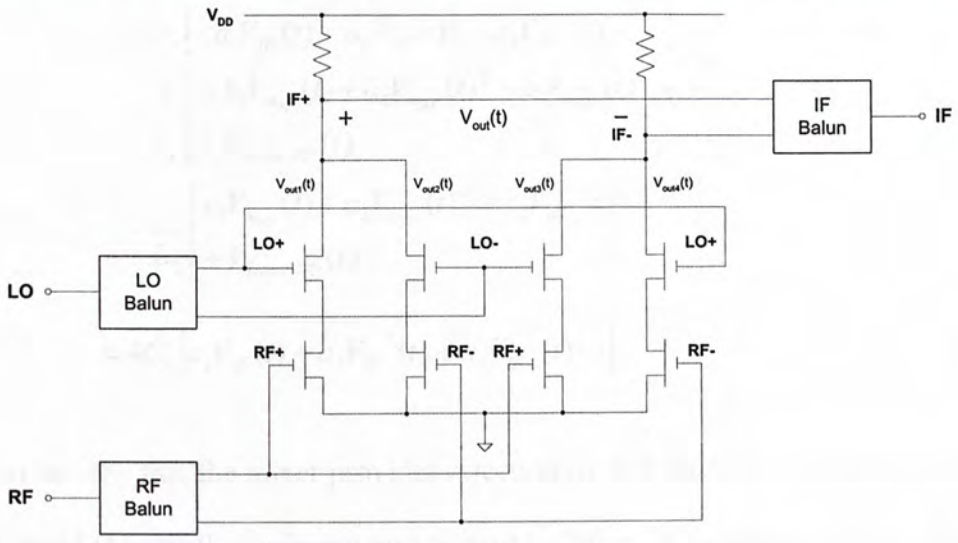

Figure 2.9 Doubly balanced dual-gate mixer

$$V_{out}(t) = V_{out1}(t) + V_{out2}(t) - V_{out3}(t) - V_{out4}(t)$$

$$\begin{aligned}
&= G_c\left[a_1 V_{IF}(t) + a_2 V_{IF}(t)^2 + a_3 V_{IF}{}^3(t) + \cdots\right] \\
&\quad + \frac{1}{L_1}\begin{bmatrix} b_1 V_{\omega_{RF}}(t) + b_2 V_{\omega_{RF}}(t)^2 + b_3 V_{\omega_{RF}}(t)^3 + \cdots \\ + V_{Noise,RF}(t) \end{bmatrix} \\
&\quad + \frac{1}{L_2}\begin{bmatrix} c_1 V_{\omega_{LO}}(t) + c_2 V_{\omega_{LO}}(t)^2 + c_3 V_{\omega_{LO}}(t)^3 + \cdots \\ + V_{Noise,LO}(t) \end{bmatrix} \\
&\quad + G_c\left[a_1 V_{IF}(t) + a_2 V_{IF}(t)^2 + a_3 V_{IF}{}^3(t) + \cdots\right] \\
&\quad + \frac{1}{L_1}\begin{bmatrix} -b_1 V_{\omega_{RF}}(t) + b_2 V_{\omega_{RF}}(t)^2 - b_3 V_{\omega_{RF}}(t)^3 + \cdots \\ + V_{Noise,RF}(t) \end{bmatrix} \\
&\quad + \frac{1}{L_2}\begin{bmatrix} -c_1 V_{\omega_{LO}}(t) + c_2 V_{\omega_{LO}}(t)^2 - c_3 V_{\omega_{LO}}(t)^3 + \cdots \\ + V_{Noise,LO}(t) \end{bmatrix} \\
&\quad - G_c\left[-a_1 V_{IF}(t) + a_2 V_{IF}(t)^2 - a_3 V_{IF}{}^3(t) + \cdots\right] \\
&\quad - \frac{1}{L_1}\begin{bmatrix} b_1 V_{\omega_{RF}}(t) + b_2 V_{\omega_{RF}}(t)^2 + b_3 V_{\omega_{RF}}(t)^3 + \cdots \\ + V_{Noise,RF}(t) \end{bmatrix} \\
&\quad - \frac{1}{L_2}\begin{bmatrix} -c_1 V_{\omega_{LO}}(t) + c_2 V_{\omega_{LO}}(t)^2 - c_3 V_{\omega_{LO}}(t)^3 + \cdots \\ + V_{Noise,LO}(t) \end{bmatrix}
\end{aligned}$$

$$
\begin{aligned}
&- G_c\left[-a_1 V_{IF}(t) + a_2 V_{IF}(t)^2 - a_3 V_{IF}{}^3(t) + \cdots\right] \\
&-\frac{1}{L_1}\begin{bmatrix} -b_1 V_{\omega_{RF}}(t) + b_2 V_{\omega_{RF}}(t)^2 - b_3 V_{\omega_{RF}}(t)^3 + \cdots \\ + V_{Noise,RF}(t) \end{bmatrix} \\
&-\frac{1}{L_2}\begin{bmatrix} c_1 V_{\omega_{LO}}(t) + c_2 V_{\omega_{LO}}(t)^2 + c_3 V_{\omega_{LO}}(t)^3 + \cdots \\ + V_{Noise,LO}(t) \end{bmatrix}
\end{aligned}
$$

$$
= 4G_c\left[a_1 V_{IF}(t) + a_3 V_{IF}{}^3(t) + a_5 V_{IF}{}^5(t)\cdots\right] \tag{2.10}
$$

It can be seen that the mixer provides rejection of AM noise, even-order distortion on both RF and LO as well as inherent port-to-port isolation. It generally requires 4 times the current consumption of an unbalanced structure topology.

2.2.5 Gilbert cell mixer

Gilbert cell mixer, or four quadrant analog multiplier was firstly proposed by B. Gilbert in 1968 [24]. Figure 2.10 shows the schematics of Gilbert cell mixer. The RF performance of Gilbert cell mixer is similar to a doubly balanced mixer including rejection of AM noise and input isolation.

In [20], P.J. Sullivan indicates that the principle mixing action of Gilbert cell mixer is caused by the switching of the upper FET between cutoff and the saturated region. In dual-gate mixer, the upper FET is operated either in the linear or saturated region. The change of MOSFET's transconductance is much greater between the cutoff and saturated region than between the linear and saturated region. Hence, Gilbert cell mixer allows a higher conversion gain to be obtained. However, the linearity is usually worse than

doubly balanced dual-gate mixer. The performance comparison between Gilbert cell mixer and doubly balanced dual-gate mixer may be found in the references [17, 20].

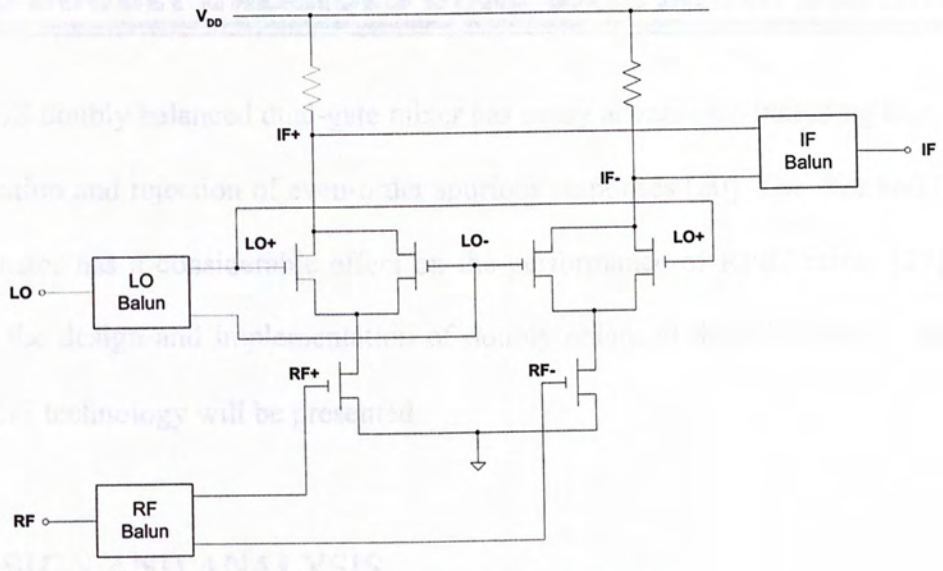

Figure 2.10 Gilbert cell mixer

CHAPTER 3

CMOS DOUBLY BALANCED DUAL-GATE MIXER DESIGN

CMOS doubly balanced dual-gate mixer has many advantages including high port-to-port isolation and rejection of even-order spurious responses [20]. The size and layout of the transistor has a considerable effect on the performance of RFIC mixer [27]. In this chapter, the design and implementation of doubly balanced dual-date mixer using 0.35 μm CMOS technology will be presented.

3.1 DESIGN AND ANALYSIS

The design of mixer based on mathematical analysis. Simulation tools can be used to verify the design. In this part, mathematical analysis on CMOS doubly balanced dual-gate mixer is depicted. The simulation results of a design example will be presented.

3.1.1 Principle of operation

Dual-gate device can be represented by using two cascade-connected single-gate FET devices [20] with equal widths. For RF application, N-channel FET device is preferred because it has higher carrier mobility for fast switching. As illustrated in Figure 3.1, the lower FET is biased for RF transconductor operation. The gate bias of the upper FET is adjusted so that the device is acting as a switch, controlled by the LO signal. The operation of the switch is described by equation (3.1).

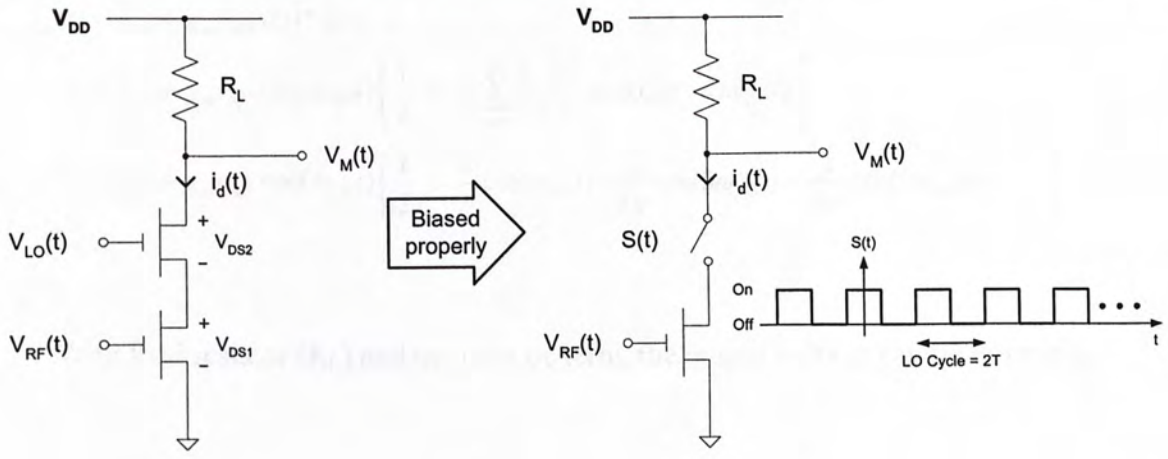

Figure 3.1 Mixing process of CMOS dual-gate mixer

$$S(t) = \begin{cases} 1 \ \text{(On)} & \ldots\ldots -\frac{T}{2} \le t \le \frac{T}{2} \\ 0 \ \text{(Off)} & \ldots\ldots -T < t < -\frac{T}{2} \ , \ \frac{T}{2} < t < T \end{cases} \qquad (3.1)$$

$$\text{with } 2T = \frac{1}{f_{LO}}$$

S(t) is a periodic square wave form with frequency f_{LO}. By using fourier series expansion, S(t) can be expressed as,

$$S(t) = \frac{1}{2} + \frac{2}{\pi}\sum_{n=0}^{\infty}\frac{(-1)^n}{2n+1}\cos((2n+1)\omega_{LO}t) \qquad (3.2)$$

If the mixing operation is assumed linear, the transistor branch current (i_d) is simply given by,

$$
\begin{aligned}
i_d(t) &= [i_{dc} + g_m V_{RF}(t)] * S(t) \\
&= [i_{dc} + g_m v_{RF} \cos(\omega_{RF} t)] \left[\frac{1}{2} + \frac{2}{\pi} \sum_{n=0}^{\infty} \frac{(-1)^n}{2n+1} \cos((2n+1)\omega_{LO} t) \right] \\
&= [i_{dc} + g_m v_{RF} \cos(\omega_{RF} t)] \left[\frac{1}{2} + \frac{2}{\pi} \cos(\omega_{LO} t) - \frac{2}{3\pi} \cos(3\omega_{LO} t) + \frac{2}{5\pi} \cos(5\omega_{LO} t) + \ldots\ldots \right]
\end{aligned}
\tag{3.3}
$$

With load resistor (R_L) and neglects dc term, the output voltage can be written as:

$$
\begin{aligned}
V_M(t) &= i_d(t) R_L \\
&= [i_{dc} + g_m v_{RF} \cos(\omega_{RF} t)] \left[\frac{1}{2} + \frac{2}{\pi} \cos(\omega_{LO} t) - \frac{2}{3\pi} \cos(3\omega_{LO} t) + \frac{2}{5\pi} \cos(5\omega_{LO} t) + \ldots\ldots \right] R_L \\
&\approx \frac{1}{2} R_L g_m v_{RF} \cos(\omega_{RF} t) && \cdots \text{RF Leakage} \\
&\quad + \frac{2}{\pi} i_{dc} \cos(\omega_{LO} t) && \cdots \text{LO Leakage} \\
&\quad + \frac{2}{\pi} R_L g_m v_{RF} \cos(\omega_{RF} t) \cos(\omega_{LO} t) && \cdots \text{Desired IF signal} \\
&\quad - \frac{2}{3\pi} R_L g_m v_{RF} \cos(\omega_{RF} t) \cos(3\omega_{LO} t) && \cdots \text{Higher harmonics} \\
&\quad + \frac{2}{5\pi} R_L g_m v_{RF} \cos(\omega_{RF} t) \cos(5\omega_{LO} t) && \cdots \text{Higher harmonics} \\
&\quad + \\
&\quad \vdots
\end{aligned}
\tag{3.4}
$$

From equation (3.4), the IF signal may be derived as,

$$
\begin{aligned}
V_{IF}(t) &= g_m v_{RF} \cos(\omega_{RF} t) R_L \left[\frac{2}{\pi} \cos(\omega_{LO} t) \right] \\
&= \frac{g_m v_{RF} R_L}{\pi} [\cos((\omega_{LO} - \omega_{RF}) t) + \cos((\omega_{LO} + \omega_{RF}) t)]
\end{aligned}
\tag{3.5}
$$

Since the lower FET operates in linear region, by using SPICE Level 1 model [25], the final output can be expressed as:

$$V_{\mathrm{IF}}(\mathrm{t}) = \mu_n C_{ox} \frac{W}{L} V_{DS1} \frac{v_{RF} R_L}{\pi} [\cos((\omega_{\mathrm{LO}} - \omega_{\mathrm{RF}})t) + \cos((\omega_{\mathrm{LO}} + \omega_{\mathrm{RF}})t)] \qquad (3.6)$$

Therefore, the conversion gain of the mixer is given by:

$$\begin{aligned} Conversion\ Gain &= \frac{|V_{IF}(t)|}{|V_{RF}(t)|} \\ &= \frac{\mu_n C_{ox} \frac{W}{L} V_{DS1} \frac{v_{RF} R_L}{\pi}}{v_{RF}} \\ &= \mu_n C_{ox} \frac{W}{L} V_{DS1} \frac{R_L}{\pi} \end{aligned} \qquad (3.7)$$

μ_n is the majority carrier mobility,

C_{ox} is gate oxide capacitance per unit area,

$\frac{W}{L}$ is transistor aspect ratio,

V_{DS1} is the lower transistor drain-to-source voltage.

Clearly, the conversion gain of the mixer can be adjusted by changing the aspect ratio $\frac{W}{L}$, the drain-to-source voltage or the load resistance value.

3.1.2 Doubly balanced dual-gate mixer

Doubly balanced dual-gate mixer basically consists of 4 dual-gate mixers. As illustrated in Figure 3.2. Both the LO and RF signals are supplied to the mixer in a differential mode. The output signal is obtained by properly combining the drain currents from the four mixer branches:

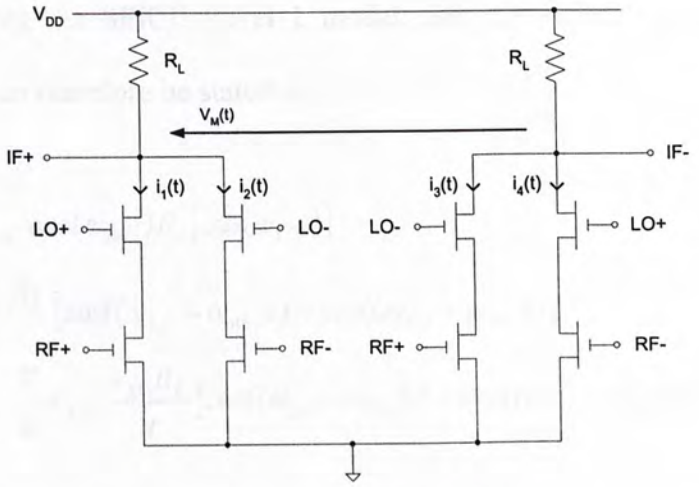

Figure 3.2 CMOS doubly balanced dual-gate mixer

$$
\begin{aligned}
V_M(t) &= \left(i_1(t) + i_2(t) - i_3(t) - i_4(t)\right)R_L \\
&= \left[i_{dc} + g_m\, v_{RF}\cos(\omega_{RF}t)\right]\left[\frac{1}{2} + \frac{2}{\pi}\sum_{n=0}^{\infty}\frac{(-1)^n}{2n+1}\cos((2n+1)\omega_{LO}t)\right]R_L \\
&\quad + \left[i_{dc} - g_m\, v_{RF}\cos(\omega_{RF}t)\right]\left[\frac{1}{2} - \frac{2}{\pi}\sum_{n=0}^{\infty}\frac{(-1)^n}{2n+1}\cos((2n+1)\omega_{LO}t)\right]R_L \\
&\quad - \left[i_{dc} + g_m\, v_{RF}\cos(\omega_{RF}t)\right]\left[\frac{1}{2} - \frac{2}{\pi}\sum_{n=0}^{\infty}\frac{(-1)^n}{2n+1}\cos((2n+1)\omega_{LO}t)\right]R_L \\
&\quad - \left[i_{dc} - g_m\, v_{RF}\cos(\omega_{RF}t)\right]\left[\frac{1}{2} + \frac{2}{\pi}\sum_{n=0}^{\infty}\frac{(-1)^n}{2n+1}\cos((2n+1)\omega_{LO}t)\right]R_L \\
&= \frac{8}{\pi}v_{RF}\, g_m R_L\cos(\omega_{RF}t)\times\left\{\cos(\omega_{LO}t) - \frac{1}{3}\cos(3\omega_{LO}t) + \frac{1}{5}\cos(5\omega_{LO}t) + \ldots.\right\} \qquad (3.8)
\end{aligned}
$$

$$
\begin{aligned}
&= \frac{8}{\pi}v_{RF}\, g_m R_L\cos(\omega_{RF}t)\cos(\omega_{LO}t) && \cdots \text{Desired IF signal} \\
&\quad - \frac{8}{3\pi}v_{RF}\, g_m R_L\cos(\omega_{RF}t)\cos(3\omega_{LO}t) && \cdots \text{Higher Harmonics} \\
&\quad + \frac{8}{3\pi}v_{RF}\, g_m R_L\cos(\omega_{RF}t)\cos(5\omega_{LO}t) && \cdots \text{Higher Harmonics} \\
&\qquad\qquad + \\
&\qquad\qquad \vdots
\end{aligned}
$$

Similarly, using the SPICE Level 1 model, the expression for the IF output and conversion gain can therefore be stated as:

$$\begin{aligned} V_{\mathrm{IF}}(t) &= \frac{8}{\pi} g_m v_{RF} \cos(\omega_{RF} t) R_L [\cos(\omega_{\mathrm{LO}} t)] \\ &= \frac{4 g_m v_{RF} R_L}{\pi} [\cos((\omega_{\mathrm{LO}} - \omega_{\mathrm{RF}})t) + \cos((\omega_{\mathrm{LO}} + \omega_{\mathrm{RF}})t)] \\ &= 4\mu_n C_{ox} \frac{W}{L} V_{DS1} \frac{v_{RF} R_L}{\pi} [\cos((\omega_{\mathrm{LO}} - \omega_{\mathrm{RF}})t) + \cos((\omega_{\mathrm{LO}} + \omega_{\mathrm{RF}})t)] \end{aligned} \tag{3.9}$$

$$Conversion\ Gain = 4\mu_n C_{ox} \frac{W}{L} V_{DS1} \frac{R_L}{\pi} \tag{3.10}$$

3.1.3 Common source output buffer

In RF measurements, we normally use 50 Ohm as the terminating impedance. If the mixer's output is connected directly to such a load, the mixing performance will be degraded. To prevent such effect, output buffer stages are therefore required.

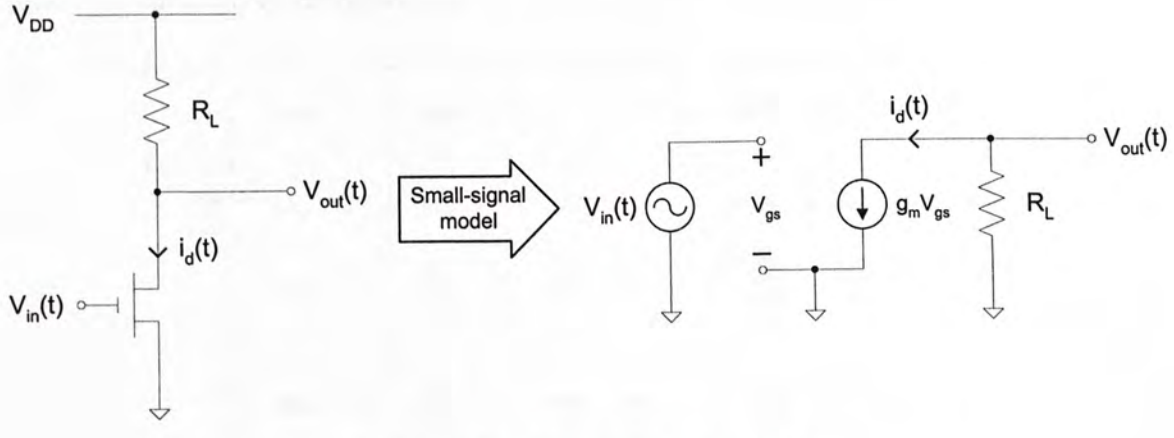

Figure 3.3 Common source output buffer

The schematic of the output buffer and its small-signal model are shown in Figure 3.3. The transistor operates in the saturation region and the corresponding output voltage can be expressed by:

$$\begin{aligned} V_{out}(t) &= -i_d(t)R_L \\ &= -g_m V_{gs} R_L \\ &= -g_m R_L V_{in}(t) \\ &= -\mu_n C_{ox} \frac{W}{L}(V_{GS} - V_{TH}) R_L V_{in}(t) \end{aligned} \tag{3.11}$$

$$\therefore \frac{V_{out}(t)}{V_{in}(t)} = -\mu_n C_{ox} \frac{W}{L}(V_{GS} - V_{TH}) R_L \tag{3.12}$$

3.1.4 Design example and simulation results

A doubly balanced dual-gate mixer was designed by using Cadence Design System. The mixer was design for 900 MHz down-conversion operation with 1 GHz LO and 2 V supply voltage. The sizes of transistor were optimized so that the mixer provides conversion gain with low current consumption and high linearity. The schematic of the mixer circuit is given in Figure 3.4.

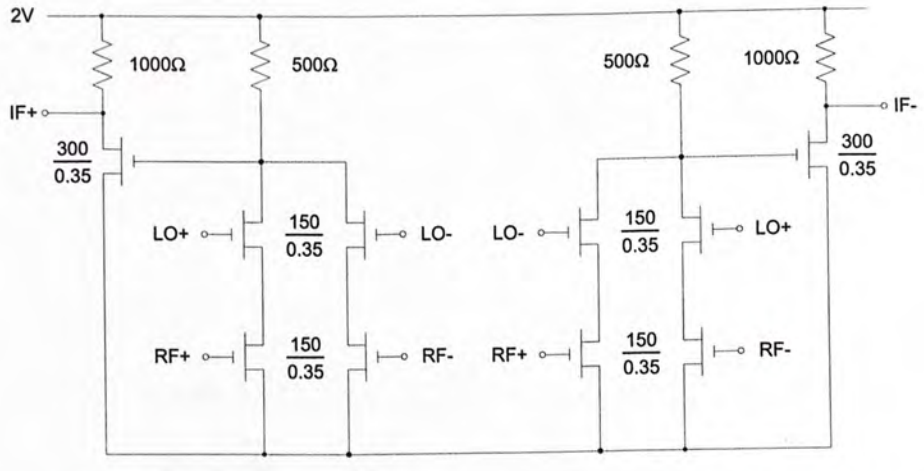

Figure 3.4 Schematic of CMOS doubly balanced dual-gate mixer with output buffer

At a LO power of –7dBm, simulation result show that the mixer provides 1.3 dB conversion gain. It has IP1dB and IIP3 of –6.34 dBm and 6.59 dBm respectively. The current consumption of the mixer and the output buffers are respectively, 3.04 mA and 2.75 mA. The simulation results are shown in Figure 3.5 to 3.8.

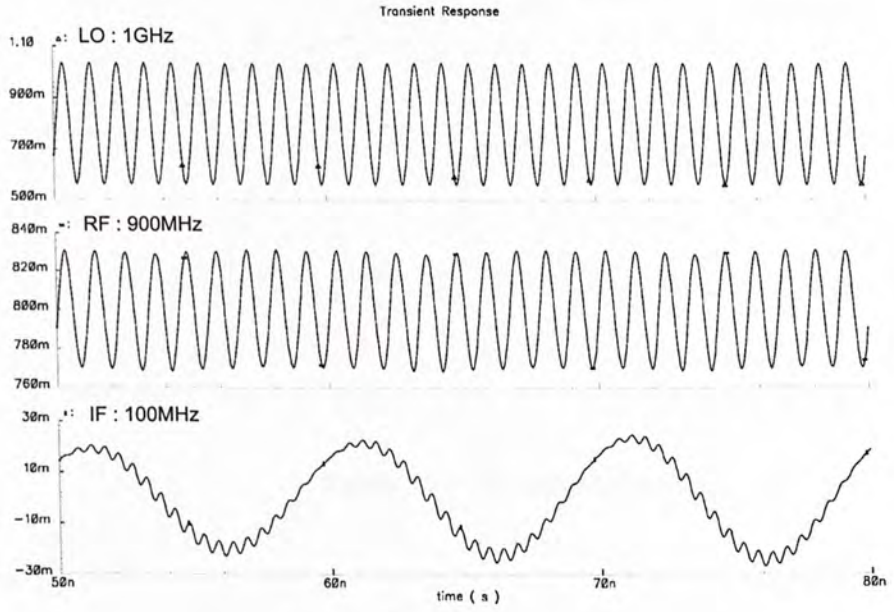

Figure 3.5 Transient response simulation result

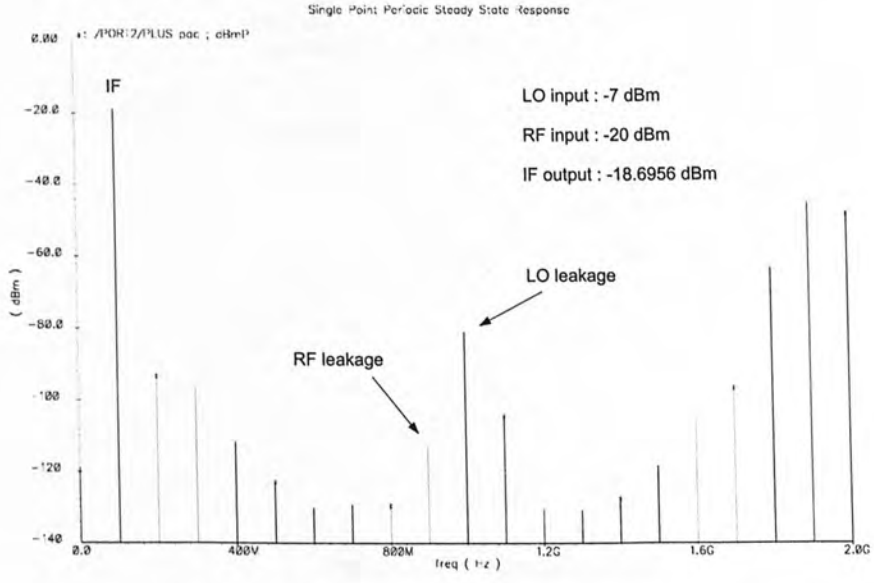

Figure 3.6 Output spectrum simulation result

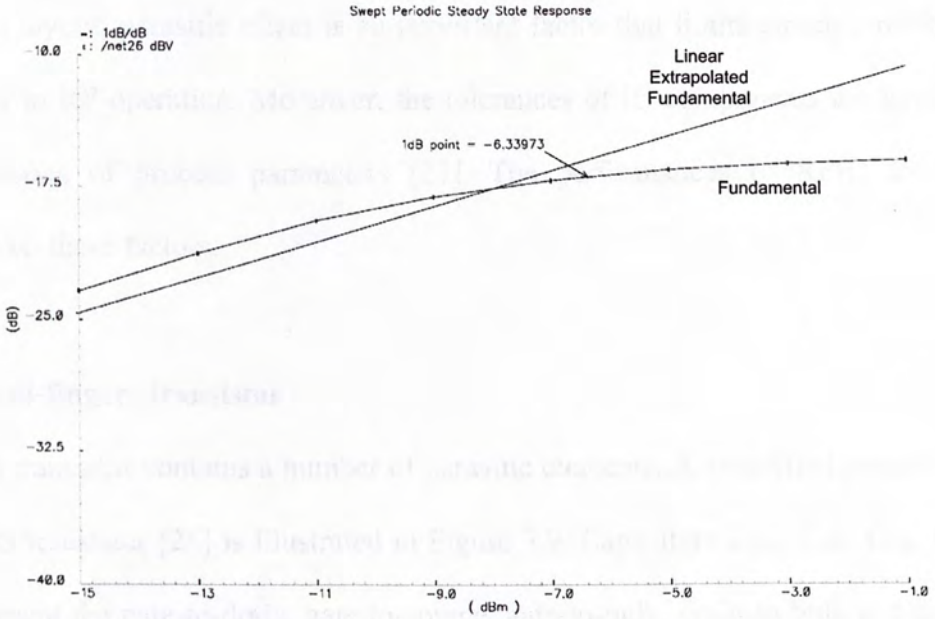

Figure 3.7 P1dB simulation result

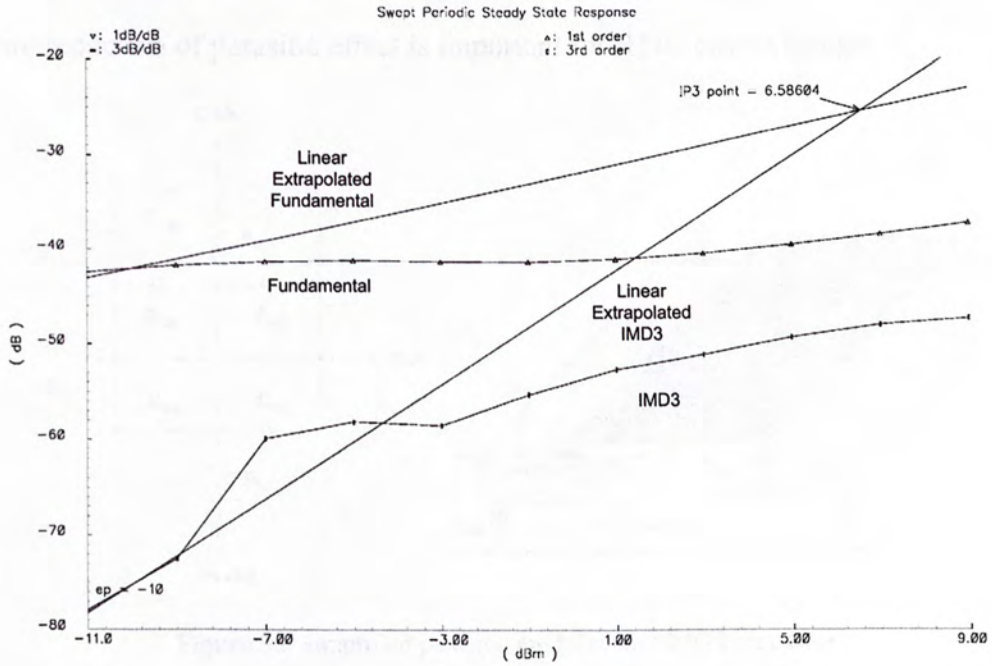

Figure 3.8 IP3 simulation result

3.2 IC LAYOUT

In the layout, parasitic effect is an important factor that limits circuit's performance especially in RF operation. Moreover, the tolerances of IC components are large due to the variations of process parameters [27]. The performances of RFIC are heavily deducted on these factors.

3.2.1 Multi-fingers transistor

MOS transistor contains a number of parasitic elements. A simplified parasitic model of NMOS transistor [26] is illustrated in Figure 3.9. Capacitors C_{GD}, C_{GS}, C_{GB}, C_{DB} and C_{SB} represent the gate-to-drain, gate-to-source, gate-to-bulk, drain-to-bulk and source-to-bulk capacitances respectively. Resistors R_G, R_S, and R_D represent the gate, source and drain resistance respectively. The parasitic elements can degrade circuit performance and therefore reduction of parasitic effect is important for RFIC circuit design.

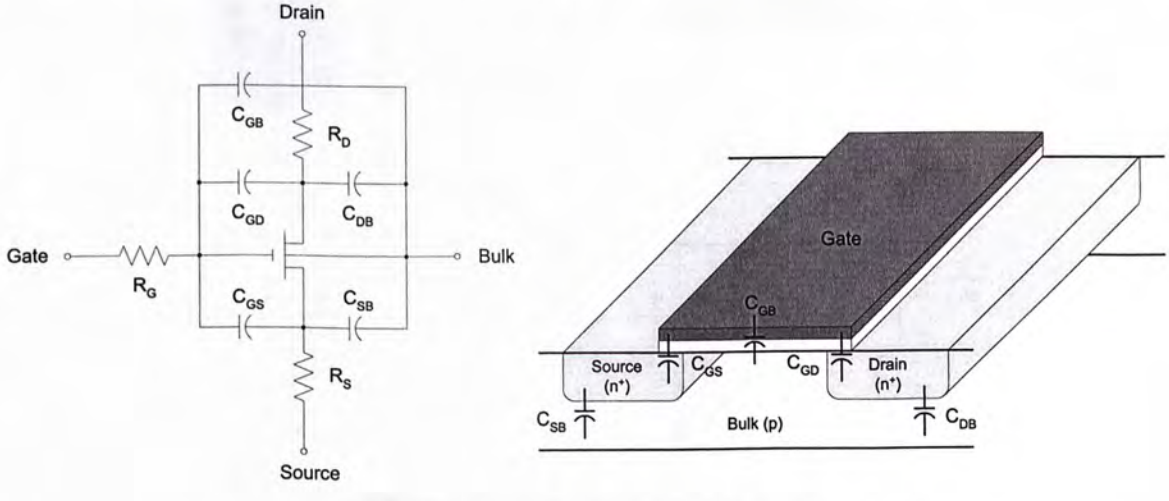

Figure 3.9 Simplified parasitic model of an NMOS transistor

For NMOS, parasitic capacitances C_{DB} and C_{SB} are proportional to the size of the n^+ diffusion region. Multi-finger structure can be applied to reduce such parasitic capacitances, as illustrated in Figure 3.10. Transistor with large aspect ratio can be divided into multiple identical sections connected in parallel. The paralleled transistors can reduce the area of diffusion region and thus parasitic capacitances are lowered. Parasitic resistances depend on the number of contact/via. At the gate, drain and source terminal, multiple contact/via is often used to reduce parasitic resistance.

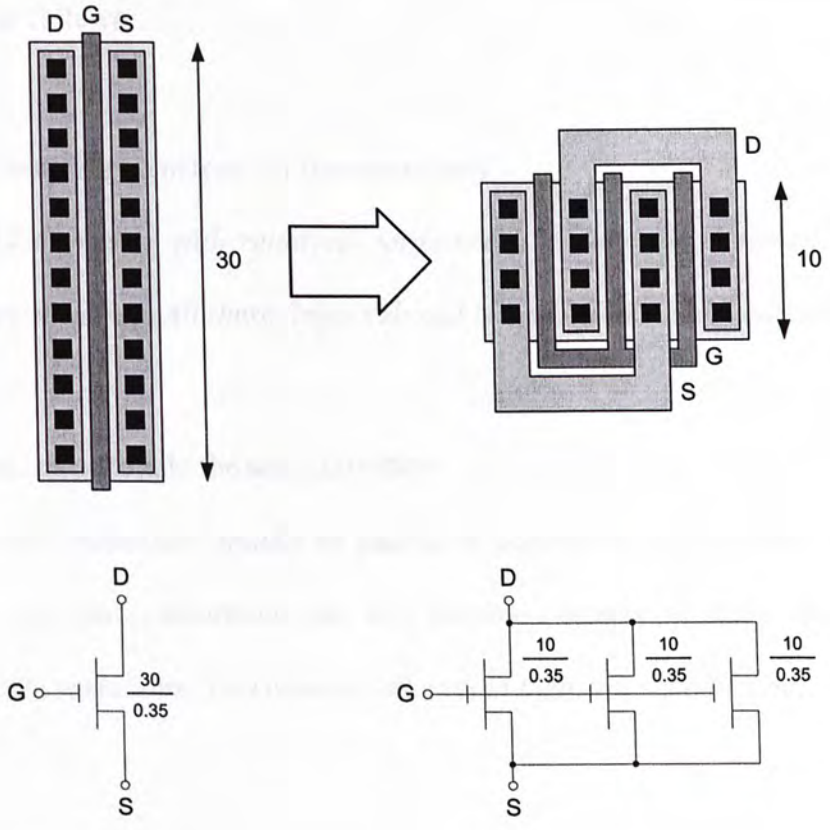

Figure 3.10 Multi-fingers transistor layout

3.2.2 Matched Transistor

In mixer designs which are based on differential pairs, circuit performances, such as rejection of LO rely on the matching of transistor electrical characteristics. The size, shape and orientation of MOS transistors affect their matching. Another important category of mismatches stems from long-range variations called gradients. The magnitude of gradient-induced mismatches depends on the separation between the effective centers of the matched device. Gradients that affect MOS matching include those of oxide thickness, stress and temperature. Precautions for designing transistors are summarized as follows:

- Use identical geometries for transistor pairs

  NMOS transistor with relatively large width is normally designed using multi-fingers structure. All these fingers should have the same width and length.

- Orient transistors in the same direction

  Matched transistors should be placed in parallel to one another. If transistors have different orientation, they will become sensitive to stress and tilt induced mobility variations. This causes variation in their transconductance values.

- Place transistors in close proximity

  Matched transistors should reside as close as possible. MOS transistors are vulnerable to gradients in temperature, stress, and oxide thickness. Transistors in close proximity reduce these gradients.

- Keep the layout of the matched transistors as compact as possible

  Matched transistors should be arranged as compact as possible. MOS transistors naturally lend themselves to long, spindly layouts that are extremely vulnerable to gradients. The only solution is compact size. This usually requires that each device be divided into a number of fingers.

3.2.3 Matched Resistor

Resistors are created by etching a doped polysilicon film. The etching rate depends on the geometry of the poly openings. Larger openings grant more access to the etchant and thus etch more quickly than small opening. Consequently, sidewell erosion occurs to a greater degree around the edges of a large opening than around the edges of a small one. This effect causes widely separated poly geometries to have smaller widths than closely packed geometries do.

When a number of polysilicon strips are arrayed side-by side, only the strips on the ends of the array experience etch rate variations. To design matched resistors, as illustrated in Figure 3.11, dummy resistors are often added to either end of an array of

matched resistors to ensure uniform etching. The spacing between the dummy segments and the adjacent resistors must match the spacing between the resistors of the array.

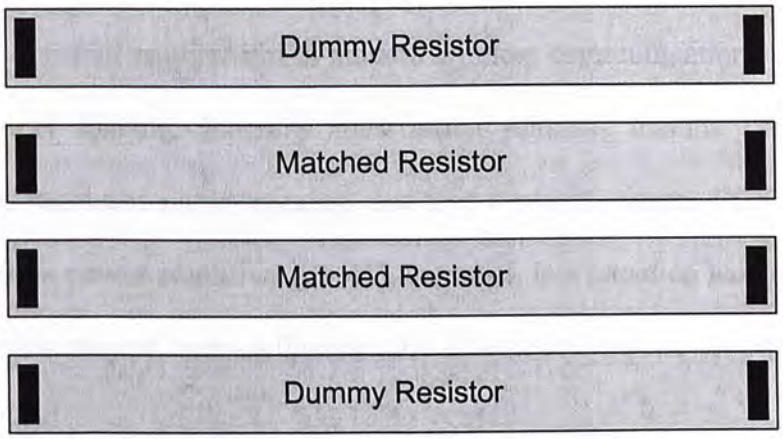

Figure 3.11 Matched array of resistors including dummies

3.2.4 Layout of CMOS doubly balanced dual-gate mixer

The IC layout of the doubly balanced dual-gate mixer in AMS 0.35 CMOS technology is shown in Figure 3.12. The IC layout techniques discussed in sections 3.2.1-3.2.3 were applied.

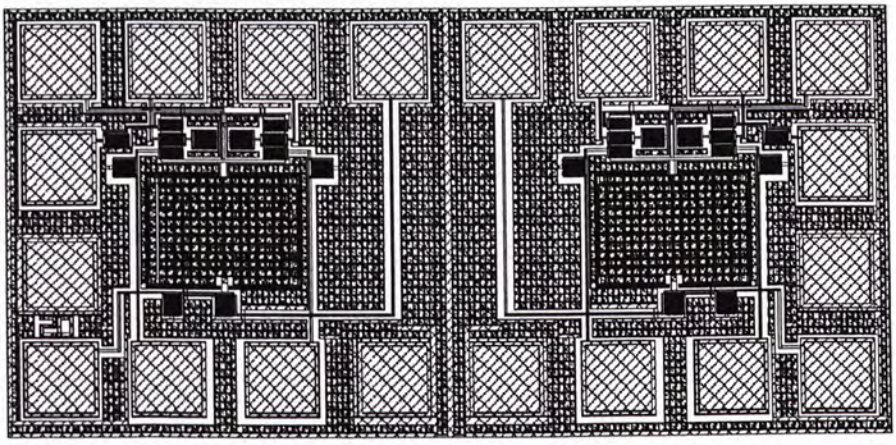

Figure 3.12 Layout of CMOS doubly balanced dual-gate mixer

CHAPTER 4

REVIEW OF MIXER LINEARIZATION TECHNIQUES

Linearity is an essential requirement in modern wireless communication systems due to the small channel spacing. Existing linearization schemes include predistortion, harmonic injection, baseband signal injection and feed-forward system. They have been studied extensively for power amplifiers [28-45], but much less attention has been paid to mixers [46-50]. In this chapter, various linearization schemes for mixers are reviewed.

4.1 SOURCE DEGENERATION

Source degeneration is the simplest approach to linearize a mixer [46]. To improve linearity, the transconductance stages are usually degenerated by an impedance Z_e. The common-emitter transconductance stage and its large-signal model are shown in Figure 4.1.

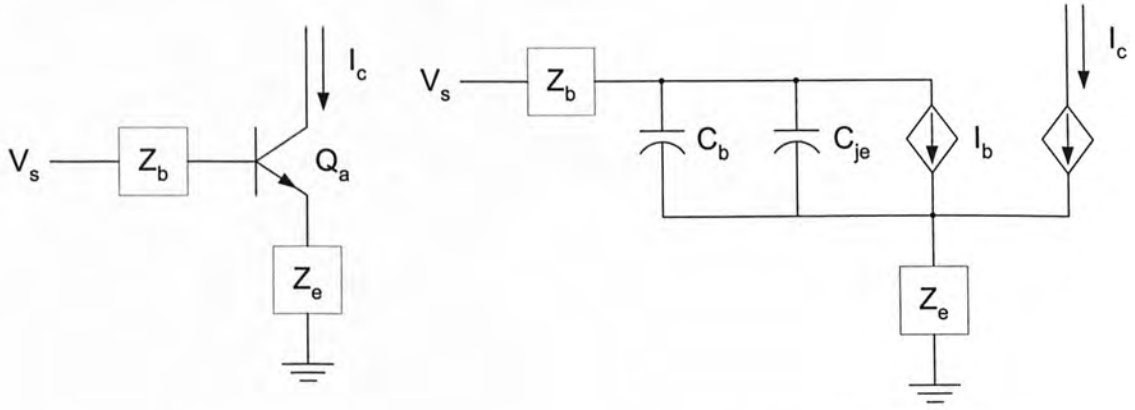

(a) (b)

Figure 4.1 Common-emitter transconductance stage (a) schematic (b) large-signal model

K. L. Fong [46] derived that the amount of IMD3 depends on the magnitude of the following expression,

$$1 + sC_{je}Z_b(s) + sC_{je}Z_e(s) \tag{4.1}$$

with inductive degeneration, the term $sC_{je}Z_e(s)$ is a complementary to the term $sC_{je}Z_b(s)$ and the magnitude of equation (4.1) will be minimized. There is no such cancellation with resistive degeneration since the term $sC_{je}Z_e(s)$ is a positive imaginary number which adds to the imaginary part of the term $sC_{je}Z_b(s)$. For the same reason, capacitive degeneration would increase the IMD3 because the term $sC_{je}Z_e(s)$ is a positive real number which adds to the "1" term. Therefore, inductors are suggested to be added at the emitters to degenerate the mixing process. The possible circuit topology is shown in Figure 4.2.

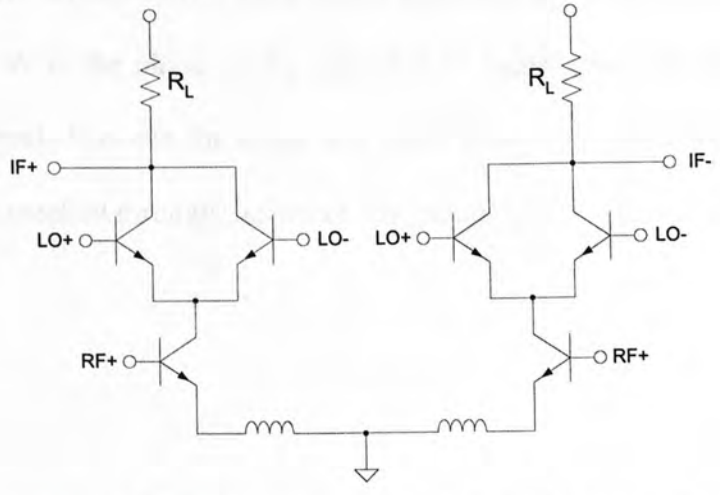

Figure 4.2 Mixer linearization by using inductive degeneration

For comparision purposes, K. L. Fong used a class AB mixer as design example [6]. Simulation predicts that the IIP3 value for inductive degeneration, resistive degeneration

and capacitive degeneration are, respectively, 3.3 dBm, 1 dBm and –2 dBm. Note that the amount of IMD reduction is rather low.

4.2 FEED-FORWARD SYSTEM

In 1998, Thomas J. Ellis described the application of feed-forward technique for mixer linearization [47]. Recently, M. Chongcheawchamnam and I.D. Robertson gave a similar but simplified version [48]. Figure 4.3 shows the schematic of the proposed simplified feed-forward system. The system has two identical mixers driven by equal RF and LO power level to provide the same output IF and IMD3. The input RF signal is equally split by using a 3 dB power divider and applied to the upper and lower branches.

The lower mixer has a smaller RF level since attenuator is added in the lower branch. So, the IF output IMD3 distortion is relatively lower than upper branch. By using a linear amplifier, the lower mixer's IMD3 level can be amplified up to the level of the IMD3 of the upper mixer. With the phase of the amplified IF signal properly adjusted by phase shifter, the IF signals between the upper and lower branch is added whereas the IMD3 components are cancelled through the use of a IF balun.

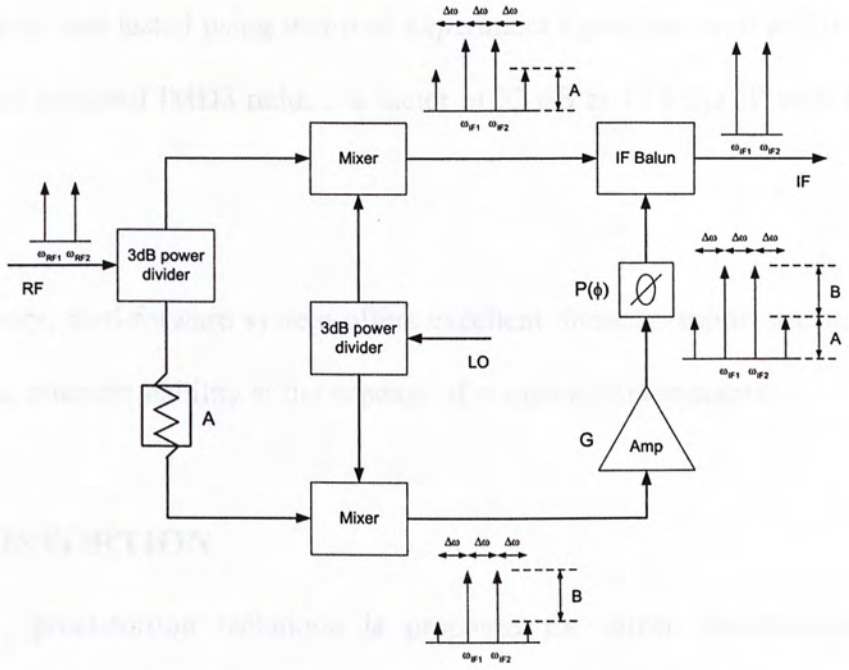

Figure 4.3 Mixer linearization by using feed-forward technique

The mixer operation can be described as a nonlinear system which can be represented by:

$$v_{mix}(x) = a_1 x + a_2 x^2 + a_3 x^3 + a_4 x^4 + a_5 x^5 + \cdots \tag{4.2}$$

When the signal $V\sin(\omega t)$ is fed to the upper mixer, it is shown elsewhere that the required amplifier gain for the cancellation of the IMD3 signal between the two branches is:

$$G = A^3\left[1+\frac{1-\frac{1}{A^2}}{\frac{4a_3}{5a_5V^2}+\frac{1}{A^2}}\right] \approx A^3 \qquad \text{if } A^2 > 5 \tag{4.3}$$

This system was tested using two-tone experiment signal centered at 2.0 and 2.0001 GHz, and had achieved IMD3 reduction factor of 32 dB at 70 MHz IF with RF input of –6.5 dBm.

In summary, feed-forward system offers excellent linearity improvement, broadband operation and inherent stability at the expense of complex implementation

4.3 PREDISTORTION

In 2002, predistortion technique is proposed for mixer linearization [49]. As illustrated in Figure 4.4, this system consists of a predistorter with nonlinear input-output characteristic $V_P(x)$ that is complementary to the nonlinear input-output characteristic $V_M(x)$ of the mixer.

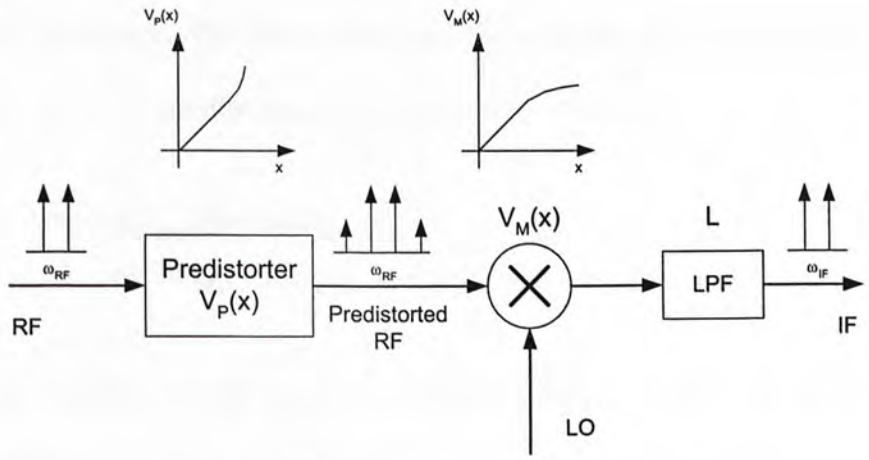

Figure 4.4 Mixer linearization by using predistortion technique

Figure 4.5 shows the predistorter which consists of a distortion-path and a delay-path. In the distortion path, an IMD error signal is generated, amplified and phase shifted by using a vector modulator. Finally, this signal is added to the delay-path signal.

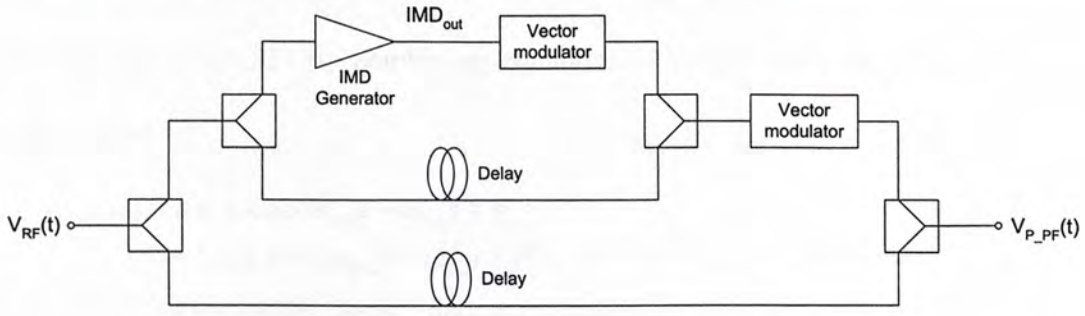

Figure 4.5 Schematic of predistorter

The output of the IMD generator can be expressed by:

$$IMD_{out}(x) = a_0 + a_1 x + a_2 x^2 + a_3 x^3 + a_4 x^4 + \cdots \tag{4.4}$$

where a_n are Taylor coefficients. if a two-tone input signal of, $x = A\cos(\omega_{RF1}t) + A\cos(\omega_{RF2}t)$ is applied to the predistorter, IMD signal will be generated. The predistorted error signal is obtained by suppressing the fundamental signal using vector modulator. This error signal and the original signal (delayed) are combined at the output. Thus the predistorted RF signal can be written as:

$$\begin{aligned} V_{P\_RF}(t) \approx\ & b_1\left[\cos(\omega_{RF1}t) + \cos(\omega_{RF2}t)\right] \\ & + b_2\left[\cos(2\omega_{RF1}t - \omega_{RF2}t + \alpha) + \cos(2\omega_{RF2}t - \omega_{RF1}t + \alpha)\right] + \cdots \end{aligned} \tag{4.5}$$

where b_n are variable, α is the phase change in vector modulator. The mixer's nonlinear output characteristic can be expressed by:

$$V_M(y) = c_0 + c_1 y + c_2 y^2 + c_3 y^3 + c_4 y^4 + \cdots \tag{4.6}$$

where c_n are Taylor coefficients of mixer and y is V_{P_RF} + LO. The IF signals from the mixer are filtered by a LPF. By combining equations (4.5) and (4.6), the output IF can now be derived as:

$$\begin{aligned} IF_{out}(t) \approx\ & b_1 c_2 L \cos(\omega_{RF1} t - \omega_{LO} t + \theta_1) \\ & + b_1 c_2 L \cos(\omega_{RF2} t - \omega_{LO} t + \theta_1) \\ & + b_2 c_2 \cos((2\omega_{RF1} - \omega_{RF2}) t - \omega_{LO} t + \theta_2) \\ & + b_2 c_2 \cos((2\omega_{RF2} - \omega_{RF1}) t) - \omega_{LO} t + \theta_2) \\ & + \frac{3}{4} b_1^{\,3} c_4 \cos((2\omega_{RF1} - \omega_{RF2}) t - \omega_{LO} t + \alpha + \theta_3) \\ & + \frac{3}{4} b_1^{\,3} c_4 \cos((2\omega_{RF2} - \omega_{RF1}) t - \omega_{LO} t + \alpha + \theta_3) \\ & + \cdots \end{aligned} \tag{4.7}$$

where θ_1, θ_2 and θ_3 are phase delay.

To a first approximation, if the amplitude and phase (α) of the pre-distorted signal is controlled properly, the down-converted IMD signal can be used to cancel the inherent IMD generated by the mixer. Consequently, the conditions for exact IMD suppression are given by:

$$\text{Amplitude condition :} \quad b_2 c_2 = \frac{3}{4} c_4 b_1^{\,3} \tag{4.8}$$

$$\text{Phase condition :} \quad \theta_2 = \alpha + \theta_3 + 180° \tag{4.9}$$

In [49], two-tone test was conducted with RF input at 836 and 836.442 MHz and 766 LO frequency. A reduction factor of 16 dB of IMD3 was reported.

This method provides moderate linearity improvement. However, the circuitry of the RF predistorter is rather complicated (especially if it is adaptive) and this method is only applicable to narrow band systems.

4.4 DIFFERENCE-FREQUENCY (LOW-FREQUENCY) INJECTION TECHNIQUE

Recently, M. Chongcheawchamnam proposed to use the difference-frequency injection technique in linearizing a doubly balanced diode mixer [50]. Figure 4.6 shows the schematic of the proposed method when applied to a microwave up-conversion mixer.

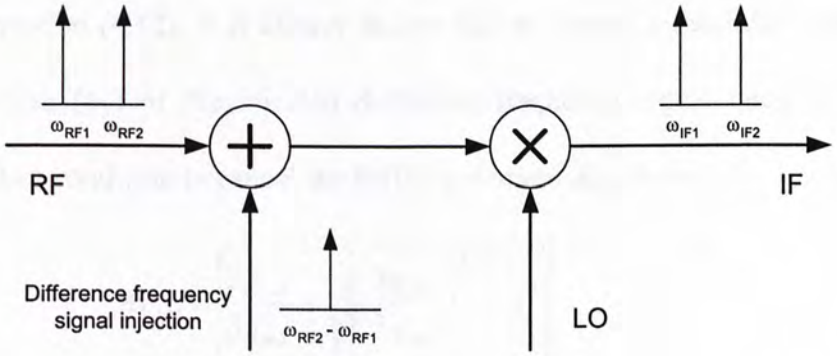

Figure 4.6 Mixer linearization by using difference-frequency injection technique

In the presence of the fundamental and the difference-frequency signals, such that.

$$V_{in}(t) = A\left[\cos((\omega_{RF1})t) + \cos((\omega_{RF2})t)\right] + A_L \cos((\omega_{RF2} - \omega_{RF1})t) \qquad (4.10)$$

Representing the nonlinearity in the mixer with a power series, the output signal of the mixer is thus given by:

$$V_{out}(t) = \sum_{k=0}^{\infty} \cos(k\omega_{LO}t) \sum_{n=0}^{\infty} g_{mn} V_{in}(t)^n \tag{4.11}$$

where g_{mn} is the n^{th}-order voltage gain which depends on the nonlinearity of the device. Assume the mixer is weakly nonlinear, the output IMD3 component can therefore be derived as:

$$\begin{aligned} IMD3 \approx & \frac{3}{4} g_{m3} \cos(\omega_{LO}t + (2\omega_{RF2} - \omega_{RF1})t) \\ & + g_{m2} A A_L \cos(\omega_{LO}t + (2\omega_{RF2} - \omega_{RF1})t - \phi_L) \\ & + \frac{3}{4} g_{m3} A A_L^{\,2} \cos(\omega_{LO}t + (2\omega_{RF2} - \omega_{RF1})t - 2\phi_L) \end{aligned} \tag{4.12}$$

From equation (4.12), it is clearly shown that to suppress the IMD3, the amplitude (A_L) and phase (ϕ_L) of the injected difference-frequency signal need to be properly controlled. The condition to cancel the IMD3 is derived as follows:

$$A_{L,opt} = \left| \frac{2g_{m2}}{3g_{m3}} + \sqrt{\left| \left(\frac{2g_{m2}}{3g_{m3}} \right)^2 - A^2 \right|} \right| \tag{4.13}$$

$$\phi_{L,opt} = \pi \qquad \text{if } A < \left| \frac{2g_{m2}}{3g_{m3}} \right|$$

or

$$= \cos^{-1}\left(\frac{2g_{m2}}{3g_{m3}} A \right) \quad \text{if } A \geq \left| \frac{2g_{m2}}{3g_{m3}} \right| \tag{4.14}$$

Mixer in doubly balanced structure may have zero quantity in even-order nonlinearity. Therefore, the optimum amplitude and phase can be further simplified as,

$$A_{L,opt} = A \tag{4.15}$$

$$\phi_{L,opt} = \frac{\pi}{2} \tag{4.16}$$

Based on the two-tone experiment with signal frequencies of 10 MHz and 10.5 MHz, an IMD3 reduction factor of 28 dB was achieved by the proposed method (LO = 1.8 GHz).

CHAPTER 5

MIXER LINEARIZATION – LOW-FREQUENCY SIGNAL INJECTION

Linearity is an essential requirement in modern wireless communication systems due to the small channel spacing. The dynamic range of a RF transceiver is often limited by the linearity performance of the low noise amplifier (LNA) and first down-conversion mixer. In this chapter, generalized low-frequency signal injection method will be introduced for linearity improvement in mixer.

5.1 MIXER'S LINEARITY

In chapter 4, the operation principle of CMOS doubly balanced dual-gate mixer was discussed. In practice, due to the device's nonlinearity, the transconductance value is a function of input voltage [51] that can be approximated by:

$$g_{m,k} = g_{m1,k} + g_{m2,k} v_{gs}(t) + g_{m3,k} v_{gs}^{\ 2}(t) \qquad (5.1)$$

Note that four distinct functions, $g_{m,k}$ (k=1,2,3,4), are employed here to account for the non-ideal mixing mechanism of different branches due to phase and amplitude imbalance of signals at the LO and RF inputs, as well as the effects of mismatch between transistors. As a result, by combing equation (3.8) and (5.1), we have:

imbalance of signals at the LO and RF inputs, as well as the effects of mismatch between transistors. As a result, by combing equation (4.8) and (5.1), we have:

$$\begin{aligned} V_M(t) = & \left[g_{m1,1}v_{gs}(t) + g_{m2,1}{v_{gs}}^2(t) + g_{m3,1}{v_{gs}}^3(t)\right]\left[\frac{1}{2} + \frac{2}{\pi}\sum_{n=0}^{\infty}\frac{(-1)^n}{2n+1}\cos((2n+1)\omega_{LO}t)\right]R_L - \\ & \left[g_{m1,2}v_{gs}(t) - g_{m2,2}{v_{gs}}^2(t) + g_{m3,2}{v_{gs}}^3(t)\right]\left[\frac{1}{2} - \frac{2}{\pi}\sum_{n=0}^{\infty}\frac{(-1)^n}{2n+1}\cos((2n+1)\omega_{LO}t)\right]R_L - \\ & \left[g_{m1,3}v_{gs}(t) + g_{m2,3}{v_{gs}}^2(t) + g_{m3,3}{v_{gs}}^3(t)\right]\left[\frac{1}{2} - \frac{2}{\pi}\sum_{n=0}^{\infty}\frac{(-1)^n}{2n+1}\cos((2n+1)\omega_{LO}t)\right]R_L + \\ & \left[g_{m1,4}v_{gs}(t) - g_{m2,4}{v_{gs}}^2(t) + g_{m3,4}{v_{gs}}^3(t)\right]\left[\frac{1}{2} + \frac{2}{\pi}\sum_{n=0}^{\infty}\frac{(-1)^n}{2n+1}\cos((2n+1)\omega_{LO}t)\right]R_L \end{aligned} \tag{5.2}$$

$$= \frac{2R_L}{\pi}\sum_{k=1}^{4}(g_{m1,k}v_{gs}(t) + g_{m2,k}{v_{gs}}^2(t) + g_{m3,k}{v_{gs}}^3(t))\left\{\cos(\omega_{LO}t) - \frac{1}{3}\cos(3\omega_{LO}t) + \frac{1}{5}\cos(5\omega_{LO}t) + \ldots.\right\}$$

where $v_{gs}(t) = v_{RF}\cos((\omega_{RF} - \frac{\Delta\omega}{2})t) + v_{RF}\cos((\omega_{RF} + \frac{\Delta\omega}{2})t)$

Subsequently, the down-converted output signal is can be expressed by*:

$$\begin{aligned} V_{IF}(t) = & \frac{1}{\pi}\sum_{k=1}^{4} g_{m1,k}v_{RF}R_L\left[\cos((\omega_{IF} - \frac{\Delta\omega}{2})t) + \cos((\omega_{IF} + \frac{\Delta\omega}{2})t)\right] \\ & + \frac{3}{4\pi}\sum_{k=1}^{4} g_{m3,k}{v_{RF}}^3R_L\left[\cos((\omega_{IF} - \frac{3\Delta\omega}{2})t) + \cos((\omega_{IF} + \frac{3\Delta\omega}{2})t)\right] \end{aligned} \tag{5.3}$$

Clearly, the output spectrum contains both the fundamental (at IF) and the third-order intermodulation distortion signal, as illustrated in Figure 5.1.

* Mathematical derivation is shown in Appendix A2

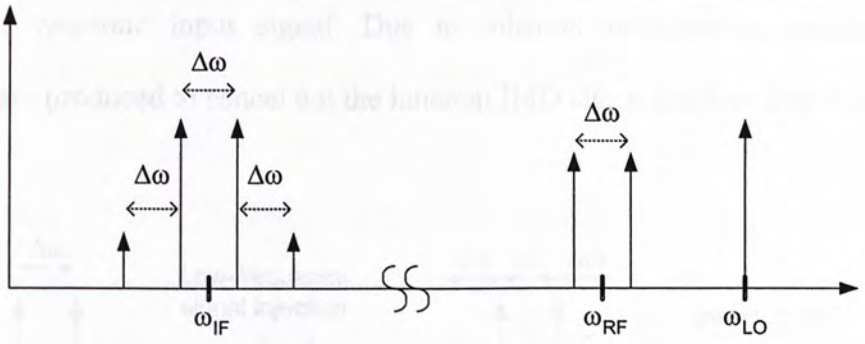

Figure 5.1 Simplified input/output spectrum

5.2 LOW-FREQUENCY SIGNAL INJECTION METHOD

A mixer has two inputs namely the LO and RF, as illustrated in Figure 5.2. In the presence of nonlinearity, IMD components will be generated at the IF output when a two-tone signal is applied to the RF input.

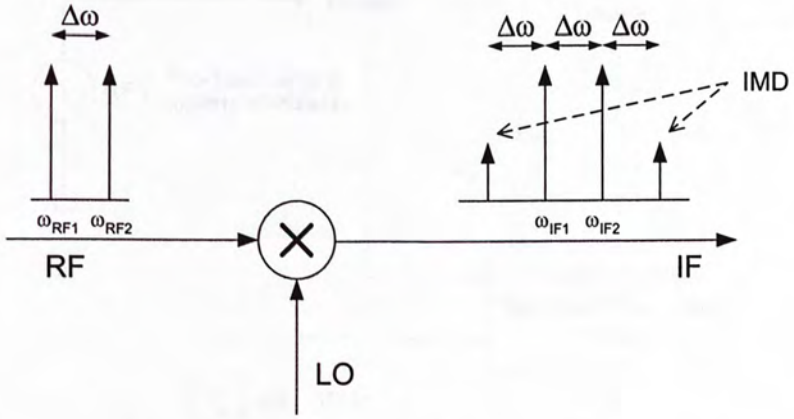

Figure 5.2 Illustration of non-ideal mixing process

In the proposed IMD suppression method, a low-frequency signal is injected into the mixer. As in Figure 5.3, the injected signal has frequency equal to the difference

frequency of two-tone input signal. Due to inherent nonlinearity, artificial IMD components are produced to cancel out the inherent IMD signal produced by the mixer.

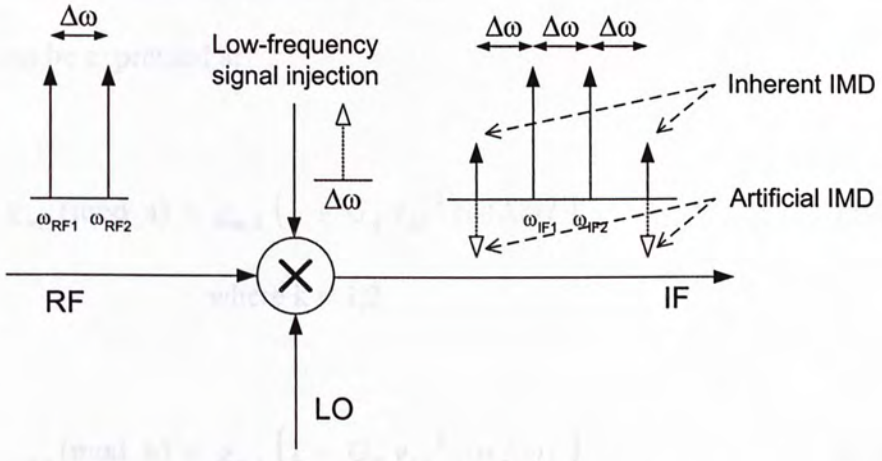

Figure 5.3 Mixer with low-frequency signal injection

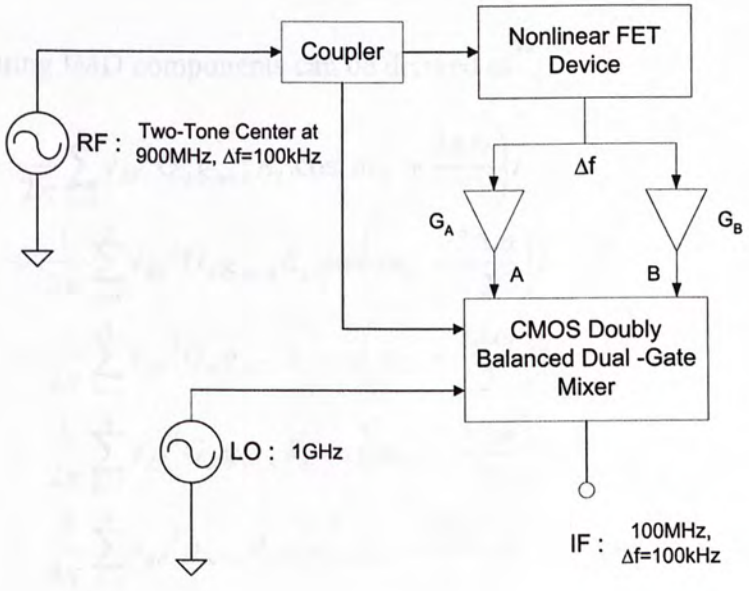

Figure 5.4 Experimental setup of low-frequency signal injection

In the practical demonstration (Figure 5.4), a portion of the two-tone input signals are coupled and fed to a FET circuitry for the extraction of the low-frequency signal from its

second-order nonlinearity. The magnitudes and polarities of the low-frequency signals are varied by two independent baseband amplifiers. Finally, these amplified signals are injected into the mixer via the drain biasing networks A and B. To a first approximation, the transconductance values of the mixer device are modulated by the low-frequency signal, which can be expressed a:

$$g_{m,k}(\text{mod\_a}) = g_{m,k}\left(1 + G_A\, v_{RF}{}^2 \cos\Delta\omega t\right) \tag{5.4}$$

where k = 1,2

$$g_{m,k}(\text{mod\_b}) = g_{m,k}\left(1 + G_B\, v_{RF}{}^2 \cos\Delta\omega t\right) \tag{5.5}$$

where k = 3,4

Hence, the resulting IMD components can be derived as**:

$$\begin{aligned} v_{IMD3}(\text{t}) = & \frac{1}{2\pi}\sum_{k=1}^{2} v_{RF}{}^3 G_A g_{m1,k} R_L \cos\left(\omega_{IF} + \frac{3\Delta\omega}{2}\right)t \\ & + \frac{1}{2\pi}\sum_{k=1}^{2} v_{RF}{}^3 G_A g_{m1,k} R_L \cos\left(\omega_{IF} - \frac{3\Delta\omega}{2}\right)t \\ & + \frac{1}{2\pi}\sum_{k=3}^{4} v_{RF}{}^3 G_B g_{m1,k} R_L \cos\left(\omega_{IF} + \frac{3\Delta\omega}{2}\right)t \\ & + \frac{1}{2\pi}\sum_{k=3}^{4} v_{RF}{}^3 G_B g_{m1,k} R_L \cos\left(\omega_{IF} - \frac{3\Delta\omega}{2}\right)t \\ & + \frac{3}{4\pi}\sum_{k=1}^{4} v_{RF}{}^3 g_{m3,k} R_L \cos\left(\omega_{IF} + \frac{3\Delta\omega}{2}\right)t \\ & + \frac{3}{4\pi}\sum_{k=1}^{4} v_{RF}{}^3 g_{m3,k} R_L \cos\left(\omega_{IF} - \frac{3\Delta\omega}{2}\right)t \end{aligned} \tag{5.6}$$

** Mathematical derivation is shown in Appendix A3

In a more compact form, the magnitude of the IMD signal may be re-written as:

$$\left|v_{IMD,L}(t)\right| = \left|v_{IMD,U}(t)\right| = {v_{RF}}^3 R_L \frac{1}{\pi}\left|\frac{1}{2}\sum_{k=1}^{2} G_A g_{m1,k} + \frac{1}{2}\sum_{k=3}^{4} G_B g_{m1,k} + \frac{3}{4}\sum_{k=1}^{4} g_{m3,k}\right|$$

$$= {v_{RF}}^3 R_L \frac{1}{4\pi}\left|\begin{array}{l} 2G_A\left(g_{m1,1}+g_{m1,2}\right)+2G_B\left(g_{m1,3}+g_{m1,4}\right) \\ +3\left(g_{m3,1}+g_{m3,2}+g_{m3,3}+g_{m3,4}\right)\end{array}\right|$$

$$= {v_{RF}}^3 R_L \frac{1}{4\pi}\left|2G_A(\alpha)+2G_B(\beta)+3(\gamma)\right| \qquad (5.7)$$

where $\alpha = g_{m1,1} + g_{m1,2}$, $\beta = g_{m1,3} + g_{m1,4}$, $\gamma = g_{m3,1} + g_{m3,2} + g_{m3,3} + g_{m3,4}$. The functions $v_{IMD,L}(t)$ and $v_{IMD,U}(t)$ denote the lower and upper IMD frequency components respectively. The above expression indicates that by properly controlling both the magnitude and polarity (G_A, G_B) of the injected signals, the artificial IMD component can be made to cancel out the inherent IMD signal.

5.2.1 Single-injection scheme

From the implementation point of view, it is simpler to apply only one injection signal ($G_A = G_B = G$). Furthermore, an IMD reduction factor may be defined as:

$$R = \frac{\left|v_{IMD}(linearized)\right|}{\left|v_{IMD}(unlinearized)\right|} = \frac{\left|2G(\alpha+\beta)+3(\gamma)\right|}{\left|3\gamma\right|} \qquad (5.8)$$

Equation (5.8) indicates that the reduction factor may be reduced by controlling the value of G properly. However, the nonlinear transconductances are not real number. Generally, single variable G is not able to simultaneously cancel both real and imaginary

part in the reduction factor. Equation (5.9) gives the optimum gain for partial cancellation of IMD signal of the single injection approach. The unsuppressed IMD component can be evaluated using equation (5.10).

$$G = -\frac{3}{2}\frac{\mathrm{Re}[\gamma]}{\mathrm{Re}[\alpha+\beta]} \tag{5.9}$$

$$R = \frac{|2G\,\mathrm{Im}(\alpha+\beta)+3\,\mathrm{Im}(\gamma)|}{|3\gamma|} \tag{5.10}$$

5.2.2 Dual-injection scheme

To have better performance on IMD suppression, two injection signals must be employed. Subsequently, an IMD reduction factor may be expressed as:

$$R = \frac{|2G_A(\alpha)+2G_B(\beta)+3(\gamma)|}{|3\gamma|} \tag{5.11}$$

Hence, by properly controlling both the magnitudes and polarities of G_A and G_B, it is possible to entirely eliminate the IMD components. The operating condition can be derived as follows:

$$2G_A(\alpha)+2G_B(\beta)+3(\gamma)=0 \tag{5.12}$$

$$\text{Where } \alpha = a_1 + jb_1 \tag{5.13}$$

$$\beta = a_2 + jb_2 \tag{5.14}$$

$$\gamma = a_3 + jb_3 \tag{5.15}$$

Since α, β and γ are complex, equation (5.12) can be re-written as:

$$2G_A a_1 + 2G_B a_2 + 3a_3 + j(2G_A b_1 + 2G_B b_2 + 3b_3) = 0 \tag{5.16}$$

By equating the real and imaginary part of the above equation to zero, we obtain:

$$2G_A a_1 + 2G_B a_2 + 3a_3 = 0 \tag{5.17}$$

$$2G_A b_1 + 2G_B b_2 + 3b_3 = 0 \tag{5.18}$$

Solving (5.17) and (5.18), we get:

$$G_A = \frac{3}{2}\frac{a_3 b_2 - a_2 b_3}{a_2 b_1 - a_1 b_2} \tag{5.19}$$

$$G_B = -\frac{3}{2}\left(\frac{a_3}{a_2} + \frac{a_3 b_2 - a_2 b_3}{a_2 b_1 - a_1 b_2} \cdot \frac{a_1}{a_2}\right) \tag{5.20}$$

5.2.3 Effect of gain error

In practice, uncertainties in gain adjustment always exist and its effect on the suppression of IMD signal can be evaluated by:

$$R = \frac{\left|2(G_{A,opt} + \Delta G_A)(\alpha) + 2(G_{B,opt} + \Delta G_B)(\beta) + 3(\gamma)\right|}{3|\gamma|} \tag{5.21}$$

where ΔG_A and ΔG_B are the corresponding gain errors. As a result, if we assume that $\frac{\Delta G_A}{G_{A,opt}} = \frac{\Delta G_B}{G_{B,opt}} = \frac{\Delta G}{G}$, the above expression can then be reduced to:

$$R = \frac{\left|2G_{A,opt}(\alpha) + 2G_{B,opt}(\beta)\right|}{3|\gamma|} \cdot \left|\frac{\Delta G}{G}\right| \approx \left|\frac{\Delta G}{G}\right| \tag{5.22}$$

Note that equation (5.22) provides a worst-case estimate of the allowable IMD reduction factor for a given value of gain error. For example, if there is 0.2 dB uncertainties in gain coefficients, the minimum achievable reduction factor can be found equal to approximately 30 dB.

5.2.4 Bandwidth limitation

In [44], it was shown that a power amplifier with memory effects exhibits third-order IMD response with both amplitude and phase that depend on the input tone spacing ($\Delta\omega$). Electrical memory effects are caused by circuit elements like capacitors and inductors used in the biasing networks, which introduce undesirable phase-shift at the signal modulation frequencies. Mathematically, the influence of memory effects on the IMD suppression capability of the dual-injection scheme can be modeled as:

$$\left|v_{IMD,U}\right| = {v_{RF}}^3 R_L \frac{1}{4\pi}\left| 2G_A e^{j\theta}(\alpha) + 2G_B e^{j\phi}(\beta) + 3(\gamma)\right| \tag{5.23}$$

$$\left|v_{IMD,L}\right| = {v_{RF}}^3 R_L \frac{1}{4\pi}\left| 2G_A e^{-j\theta}(\alpha) + 2G_B e^{-j\phi}(\beta) + 3(\gamma)\right| \tag{5.24}$$

where θ and ϕ represent the frequency-dependent phase-shift introduced by the biasing circuitry. It is clear that complete cancellation of both the upper and lower IMD components is impossible. It was also proven in [45] that significant reactive biasing impedance at signal modulation frequencies can produce asymmetrical IMD spectrum in amplifiers. For purposes of analysis, by applying the small angle approximation and the optimum gain condition in (5.19) and (5.20), equations (5.23) and (5.24) can be simplified as:

$$\left|v_{IMD,U}\right| \approx \left|v_{IMD,L}\right| \approx {v_{RF}}^3 R_L \frac{1}{2\pi}\left|j\theta G_{A,opt}(\alpha) + j\phi G_{B,opt}(\beta)\right| \tag{5.25}$$

It is also reasonable to assume that the amount of phase-shift introduced by the biasing networks are similar (θ=β=δ), and subsequently the IMD reduction factor may be re-stated as:

$$R = \frac{\left|2G_{A,opt}(\alpha) + 2G_{B,opt}(\beta)\right|}{3|\gamma|} \cdot |\delta| \approx |\delta| \tag{5.26}$$

And to account for the unsuppressed IMD signal due to the presence of gain error and higher-order mixing products, equation (5.26) may be modified as:

$$R'(\delta) = \left|\delta + \frac{i_{IMD}(unsuppressed)}{\left|i_{IMD}(unlinearized)\right|}\right| \tag{5.27}$$

where $R'(\delta)$ is the realizable IMD reduction factor with memory effects. Under the worst-case consideration, the IMD components are added in-phase to give:

$$R'(\delta) = |\delta| + R'(0) \tag{5.28}$$

where $R'(0)$ is the attainable IMD reduction factor with no memory effects. Figure. 5.5 shows the predicted suppression degradation of the proposed method as a function of the phase-shift introduced. In practice, electrical memory effects can be minimized by the careful design of the biasing circuit impedance at the signal modulation frequencies.

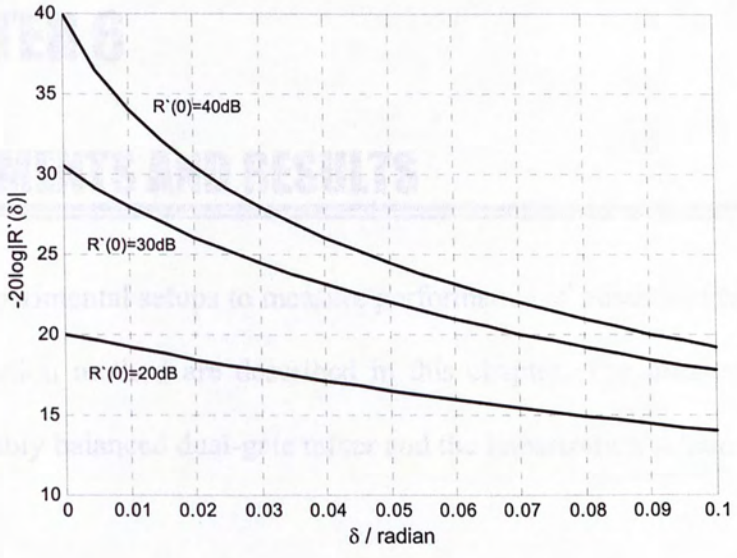

Figure 5.5 Degradation of IMD reduction factor versus low-frequency phase-shift

CHAPTER 6

EXPERIMENTS AND RESULTS

The experimental setups to measure performance of mixer and test the low-frequency signal injection method are described in this chapter. The measurement results of the CMOS doubly balanced dual-gate mixer and the linearization schemes are presented.

6.1 CMOS DOUBLY BALANCED DUAL-GATE MIXER

Figure 6.1 shows the microphotograph of the mixer fabricated using 0.35μm CMOS process. The circuit had an active area of less than 300 × 250 μm^2. In Figure 6.2, the mixer chip was mounted and wire-bonded onto a standard printed circuit board (FR4). The RF, IF and LO signals were fed differentially from off-chip passive balun. The LO and RF signals were obtained from HP 8648C signal generators and the output IF spectrum was then observed on an HP 8546A EMI receiver. For the noise figure measurement, HP 8970C noise figure meter with HP 346B noise source were used.

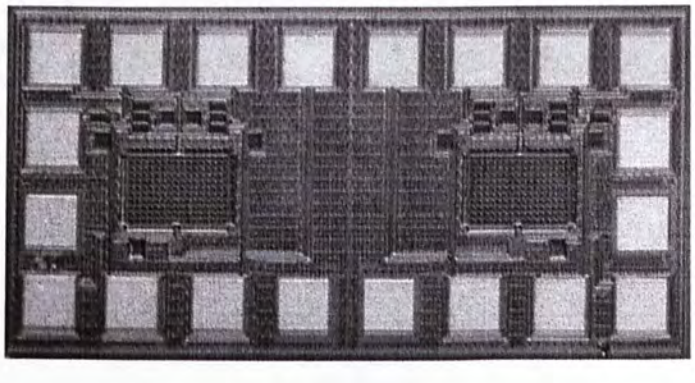

Figure 6.1 Microphotograph of CMOS mixer chip

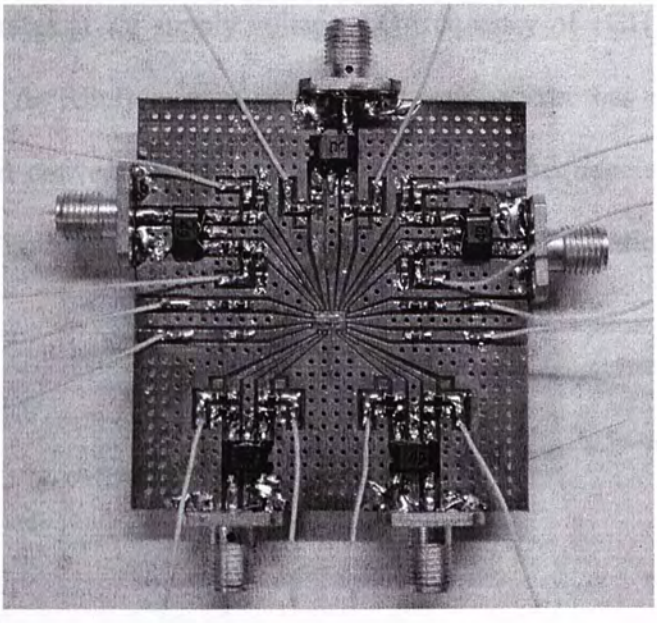

Figure 6.2 CMOS Mixer testing board

6.1.1 Conversion gain

The measurement setup for conversion gain determination is shown in Figure 6.3. The mixer was properly biased and driven using optimum LO power. Conversion gain of mixer was extracted from the measured RF input and IF output power level readings.

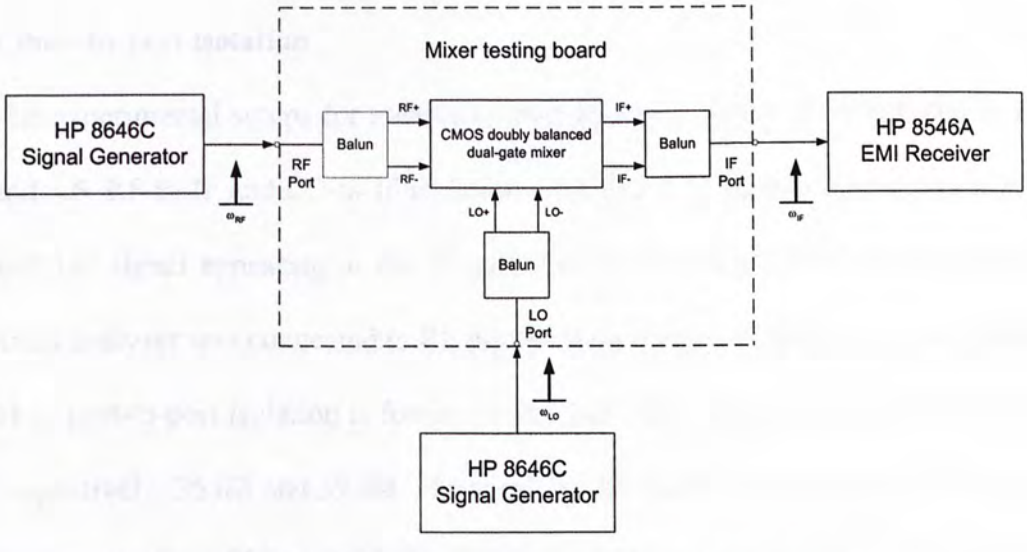

Figure 6.3 Experimental setup for conversion gain measurement

The mixer operates at 2V supply voltage, LO frequency of 1GHz and optimum LO power of –5dBm. At RF frequency of 900 MHz, the mixer has conversion gain of –6.43dB. Measured conversion gain for the range of RF frequencies from 850 to 950 MHz is given in Figure 6.4. The entire mixer and buffer combination consumes a total current of 3.6mA

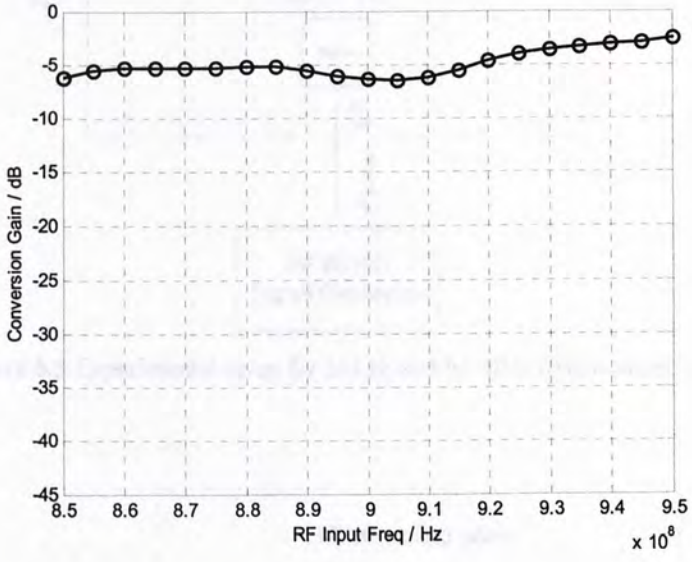

Figure 6.4 Conversion gain versus RF frequency

6.1.2 Port-to-port isolation

The experimental setups for measuring port-to-port isolation are illustrated in Figure 6.5 and 6.6. RF-to-IF and LO-to-IF isolation were found by measuring the power level of RF and LO signal appearing at the IF port. For determining the LO-to-RF isolation, a spectrum analyzer was connected to RF port to observe the LO leakage power. More than 35 dB of port-to-port isolation is found. At 900 MHz RF, The RF-IF and LO-IF isolation are, respectively, 35 dB and 39 dB. Measured RF-IF and LO-IF isolation for the range of RF frequencies from 850 to 950 MHz is given in Figure 6.7 (a). The LO-RF isolation is

43 dB at 900 MHz LO. Measured LO-RF isolation is frequency range from 850 to 950 MHz is provided in Figure 6.7 (b).

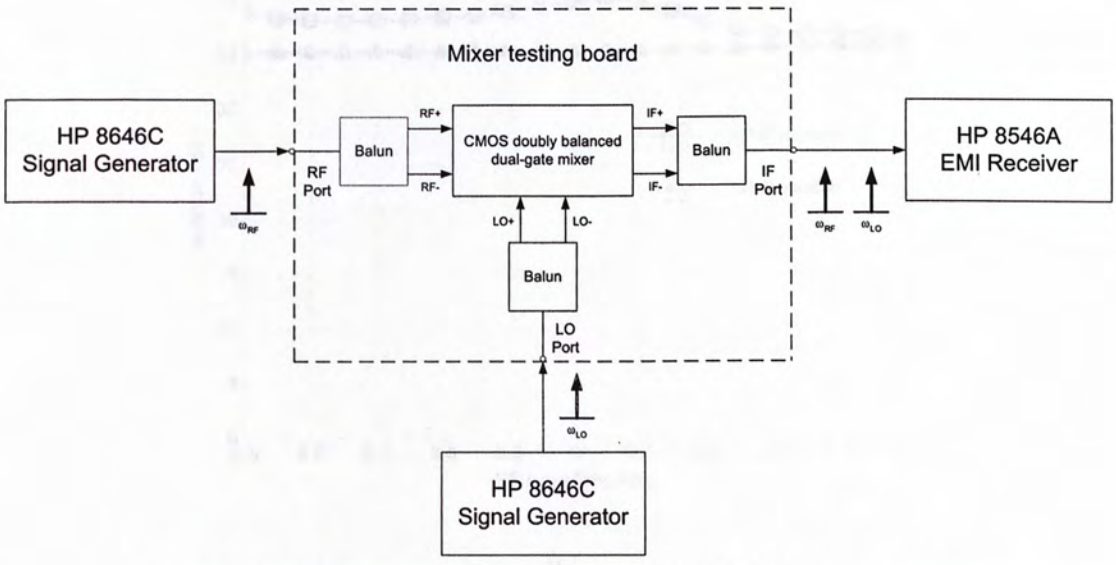

Figure 6.5 Experimental setup for LO-IF and RF-IF isolation measurement

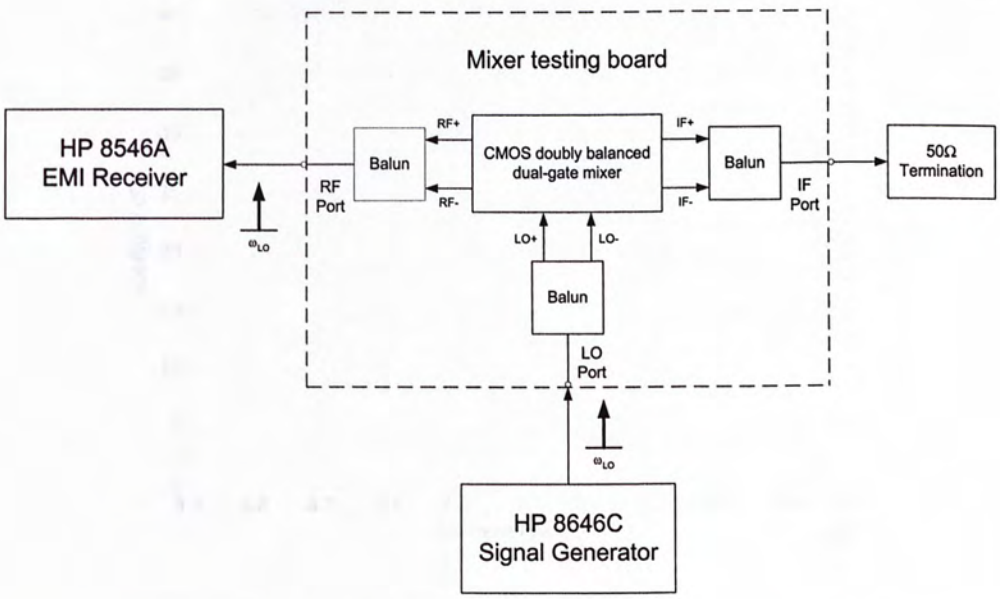

Figure 6.6 Experimental setup for LO-RF isolation measurement

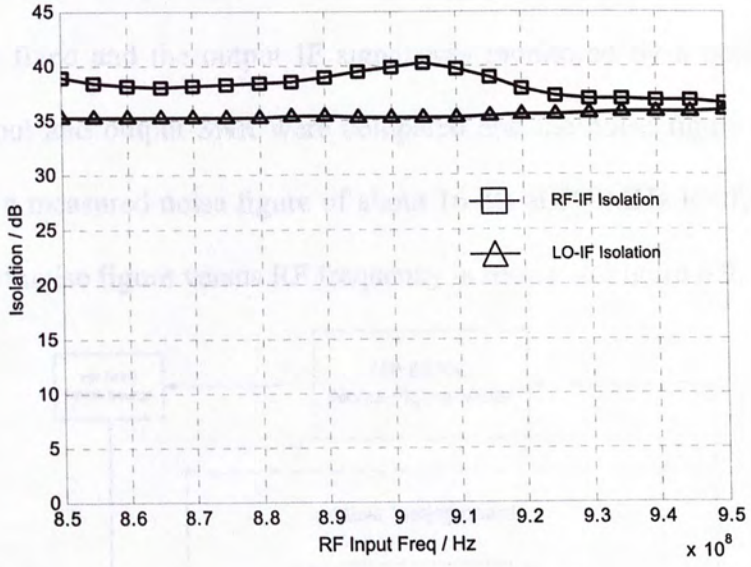

(a)

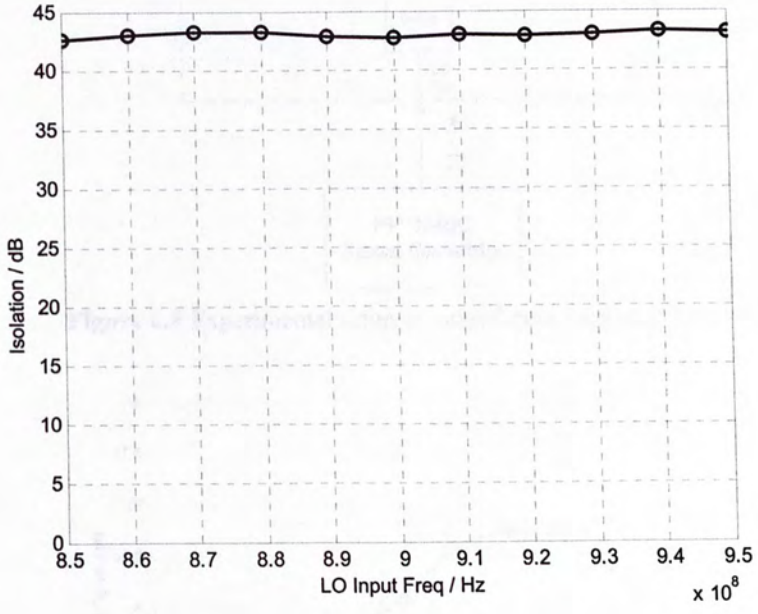

(b)

Figure 6.7 Port-to-port isolation versus frequency (a) RF-IF and LO-IF isolation (b) LO-RF isolation

6.1.3 Noise figure

The experimental setup for noise figure measurement is depicted in Figure 6.8. The LO signal was fixed and the output IF signal was monitored by a noise figure meter. Finally, the input and output SNR were compared and the noise figure was calculated. The mixer has a measured noise figure of about 16 dB at 900MHz RF frequency. Swept measurement of noise figure versus RF frequency is shown in Figure 6.9.

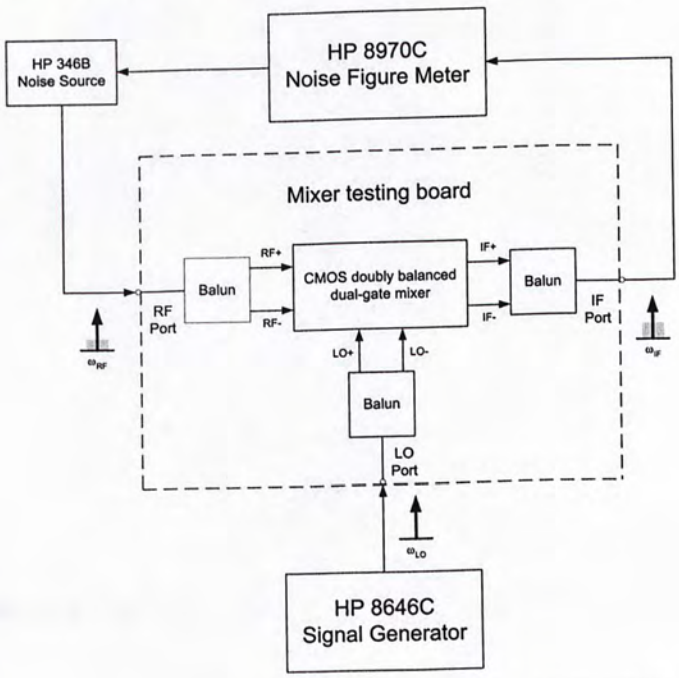

Figure 6.8 Experimental setup of noise figure measurement

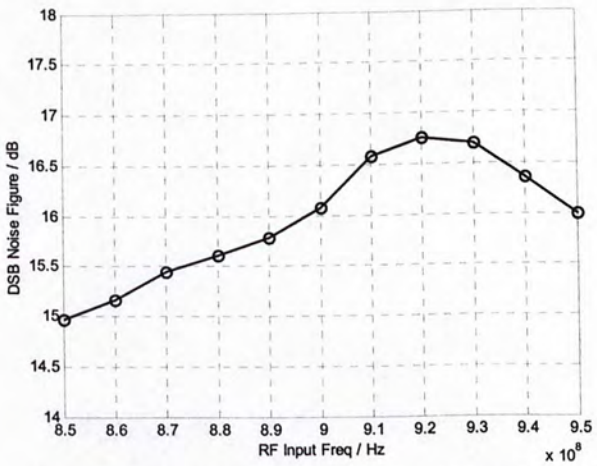

Figure 6.9 DSB noise figure versus RF frequency

6.1.4 1-dB compression point

Figure 6.10 shows the experimental setup for obtaining the 1-dB compression point of the mixer. The 1-dB compression point was extracted from the plot of IF output power versus RF input power while the input RF power was varied from –40 dBm to 0 dBm, and keeping the LO power fixed at –7 dBm (Figure 6.11). At 900MHz RF, the input P1dB is –5 dBm from measurement.

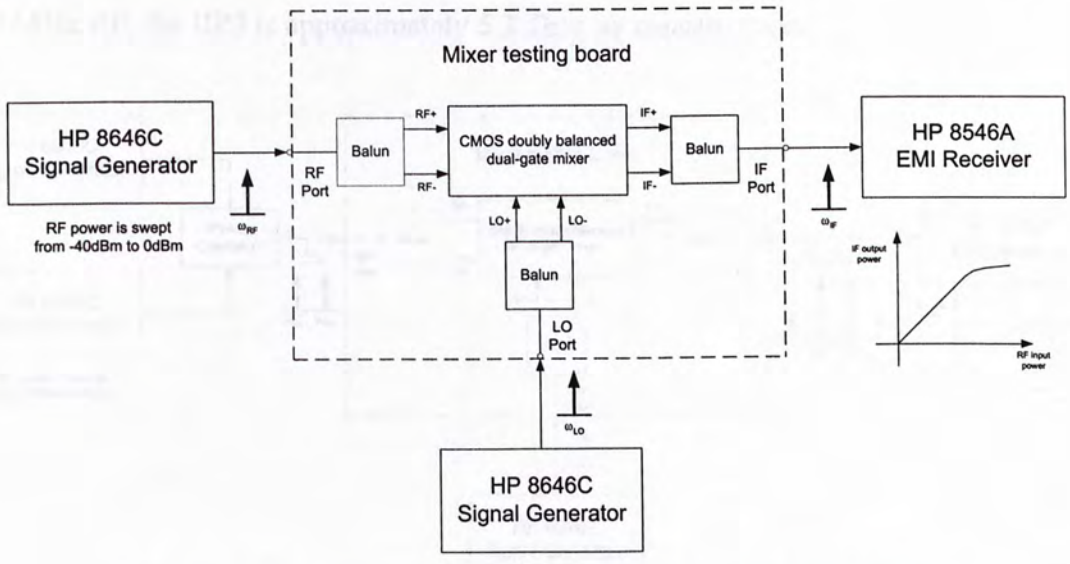

Figure 6.10 Experimental setup of 1-dB compression point measurement

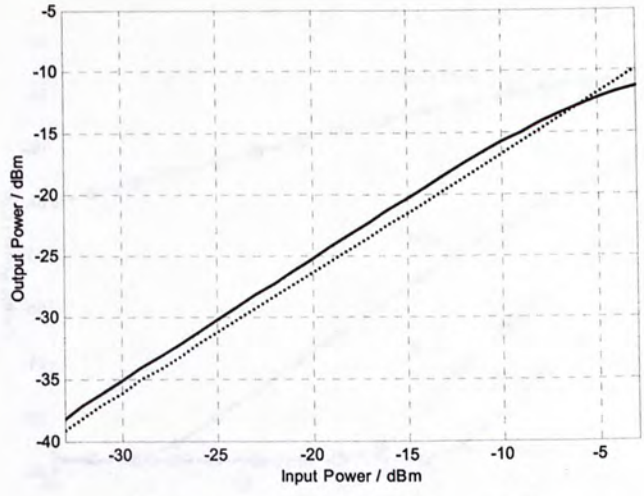

Figure 6.11 IF output power versus RF input

6.1.5 3rd -order intercept point

The experimental setup for determining the 3rd order intercept point is given in Figure 6.12. Two-tone test signal was obtained by using two HP 8648C signal generators. These signals were combined using a power-combiner and fed to the RF input of the mixer. The 3rd order intercept point was found by extrapolation from the plot of he measured IMD level (IF) with RF input power varying form –35dBm to 0 dBm (Figure 6.13). At 900 MHz RF, the IIP3 is approximately 5.3 dBm by measurement.

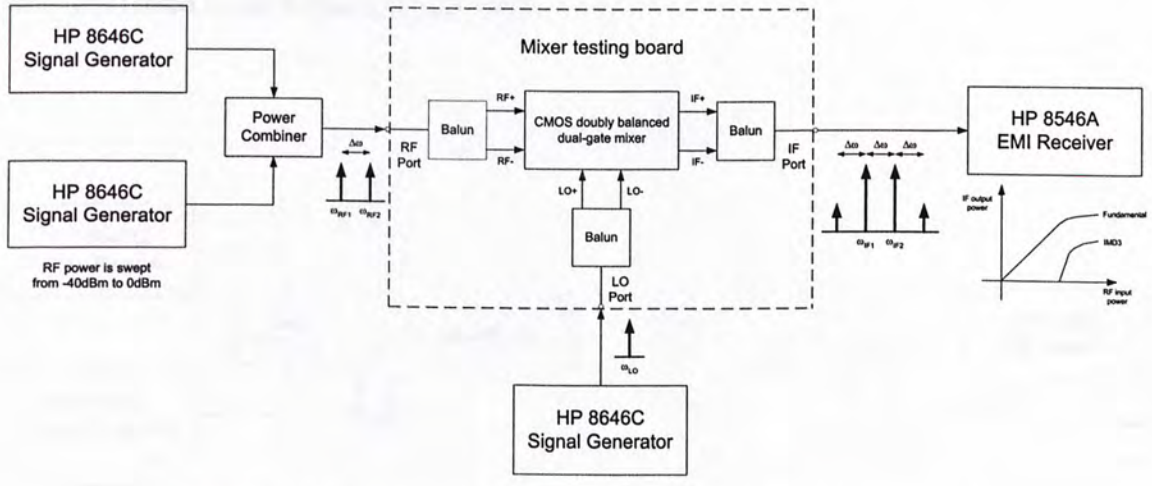

Figure 6.12 Experimental setup of 3rd order intercept point measurement

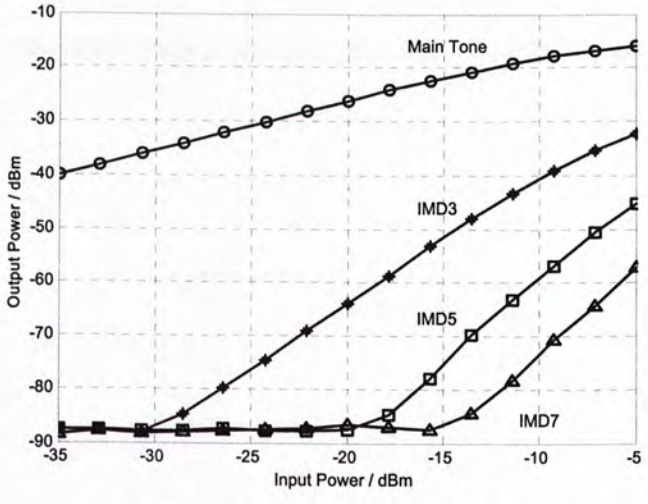

Figure 6.13 Mixer's non-linear behaviors

6.2 LOW-FREQUENCY SIGNAL INJECTION METHOD

Figure 6.14 and 6.15 show the experimental setup for both single and dual low-frequency signal injection schemes. Two-tone measurement was conducted using signals centered at 900 MHz with a frequency spacing of 100 kHz. The two-tone signal was fed to a coupler and a portion of the signal was fed to FET circuitry for the generation of the low-frequency signal. The low-frequency signal level was then amplified by baseband amplifiers before feeding to the mixer through the drain biasing network. The IF output was monitored using a spectrum analyzer.

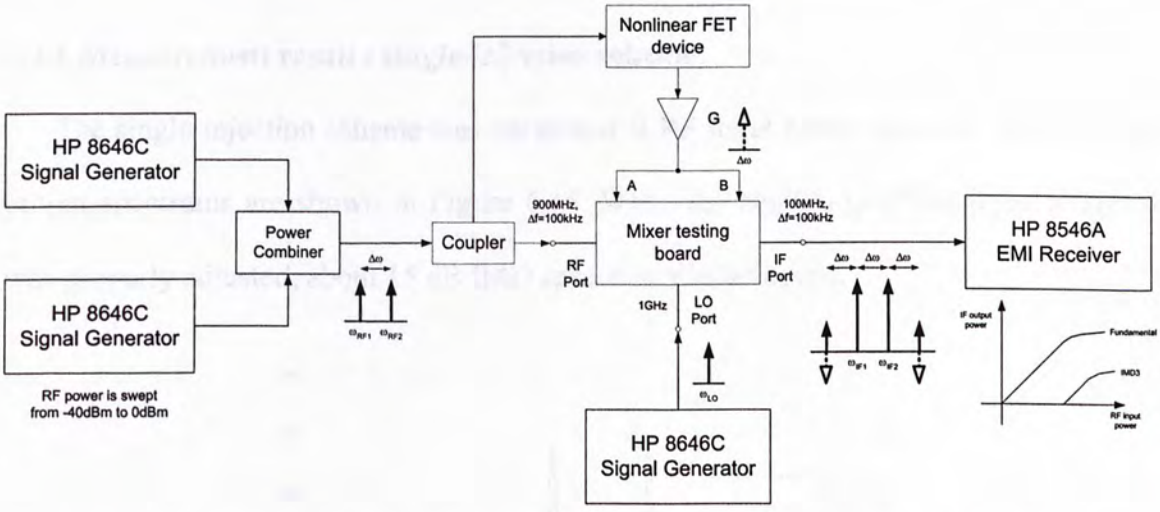

Figure 6.14 Experimental setup of low-frequency signal injection – single injection scheme

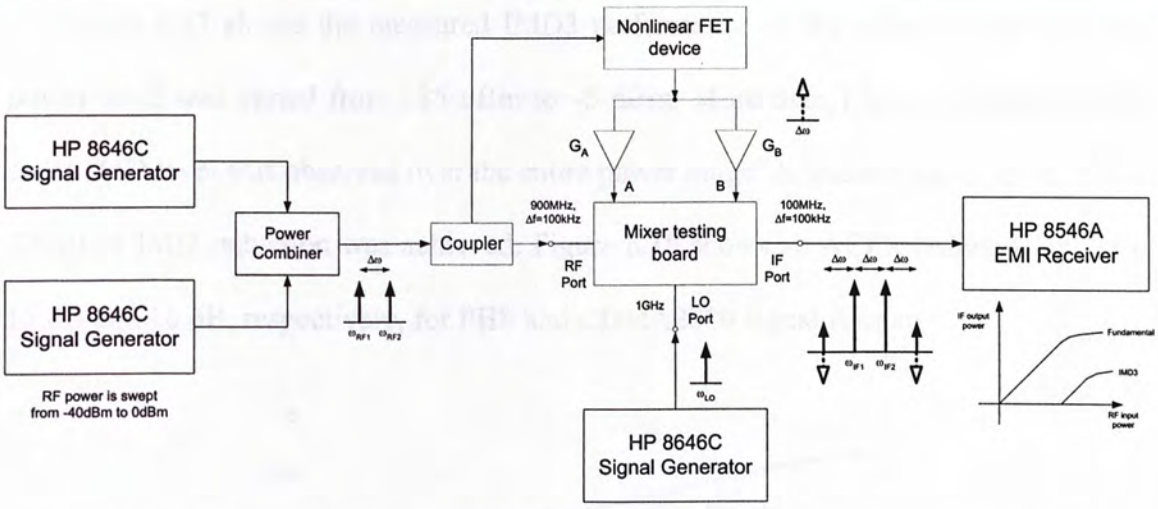

Figure 6.15 Experimental setup of low-frequency signal injection – dual injection scheme

6.2.1 Measurement result : single-injection scheme

The single injection scheme was optimized at RF input power level of –17dBm. The output spectrums are shown in Figure 6.16. When the amplitude of the injected signal was properly adjusted, about 15 dB IMD reduction was achieved.

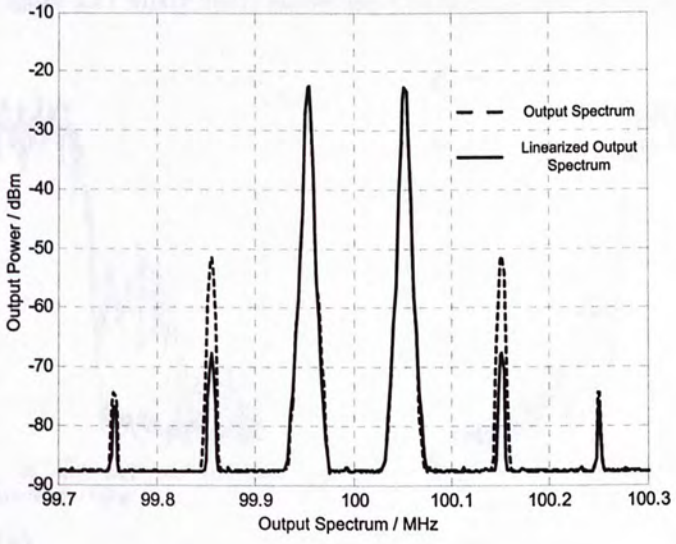

Figure 6.16 Mixer output spectrums before and after linearized

Figure 6.17 shows the measured IMD3 performance of the mixer, as the RF input power level was varied from –35 dBm to –5 dBm. More than 15dB reduction in third-order IMD level was observed over the entire power range. At certain power level, almost 20 dB of IMD reduction was achieved. Figure 6.18 shows an ACPR reduction factor of 15 dB and 10 dB, respectively, for PHS and CDMA2000 signal formats.

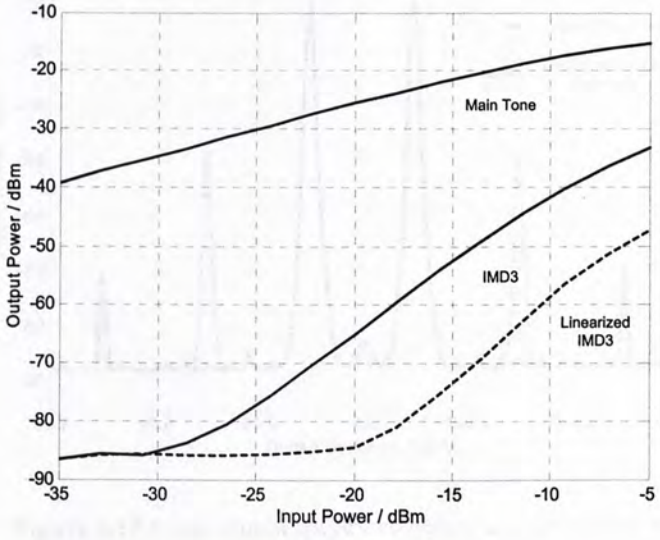

Figure 6.17 Mixer IMD3 performance before and after linearized

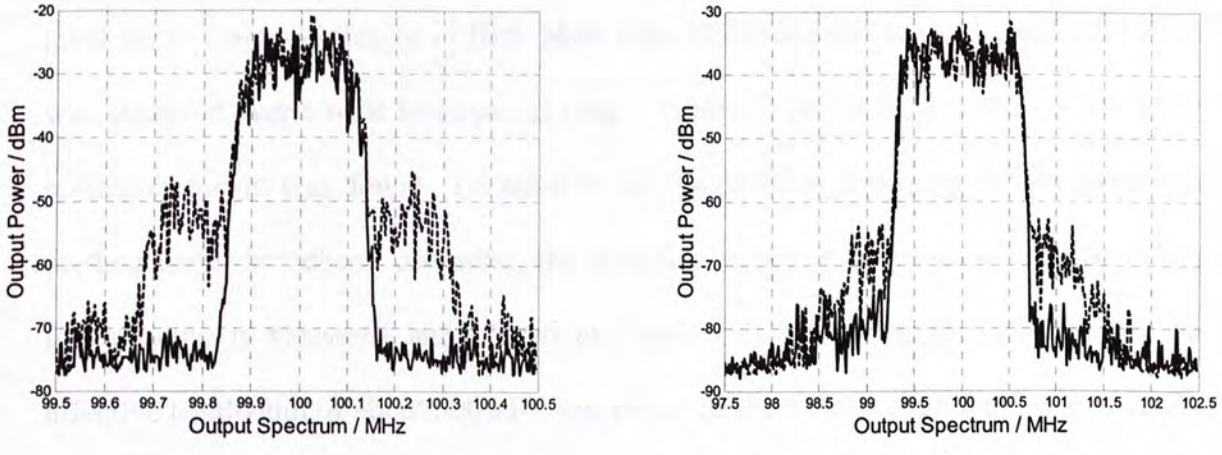

Figure 6.18 Vector-modulated signal test (a) PHS (b) CDMA2000

6.2.2 Measurement result : dual-injection scheme

The dual injection scheme was optimized at RF input power level of –15dBm. The output spectrums are shown in Figure 6.19. When the amplitudes of the injected signals were properly adjusted, about 38 dB IMD reduction was achieved.

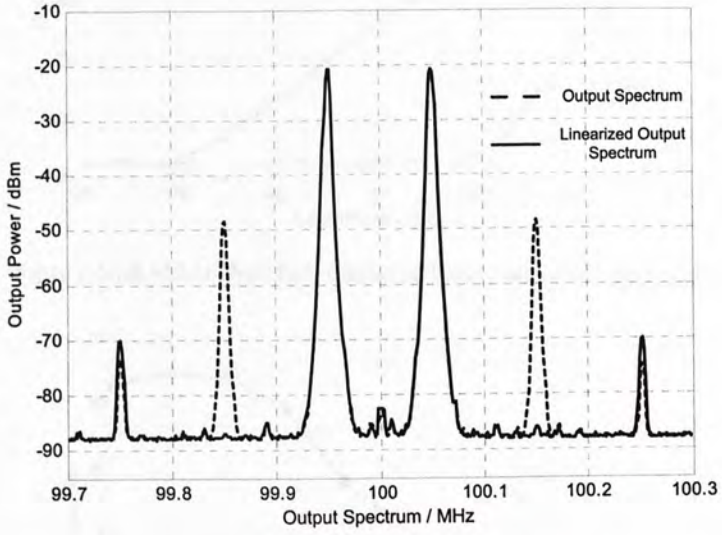

Figure 6.19 Mixer output spectrums before and after linearized

Figure 6.20 shows the measured mixer's IMD3 performance as the RF input power level varies from –35dBm to –5dBm. More than 30dB reduction in third-order IMD level was observed over a wide input power range. At certain power level, almost 40 dB IMD reduction factor was found. To observe the suppression capability of the proposed method under broadband operation, the reduction factor of IMD3 as a function of the tone-spacing is measured and plotted in Figure 6.21. The diagram indicates that an effective bandwidth of about 500 kHz was observed for a IMD reduction factor of 25dB. Figure 6.22 shows an ACPR reduction factor of 20 dB and 15 dB, respectively, for PHS and CDMA2000 signal format.

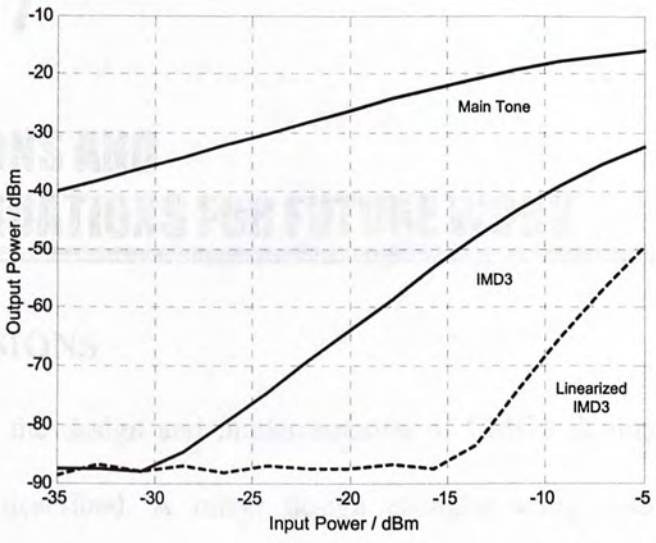

Figure 6.20 Mixer IMD3 performance before and after linearized

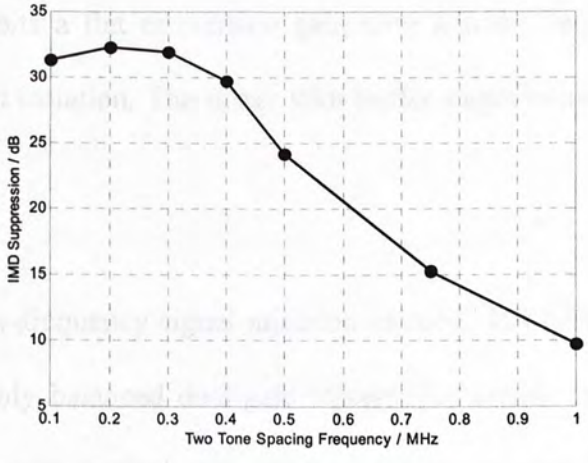

Figure 6.21 IMD Suppression versus two tone spacing

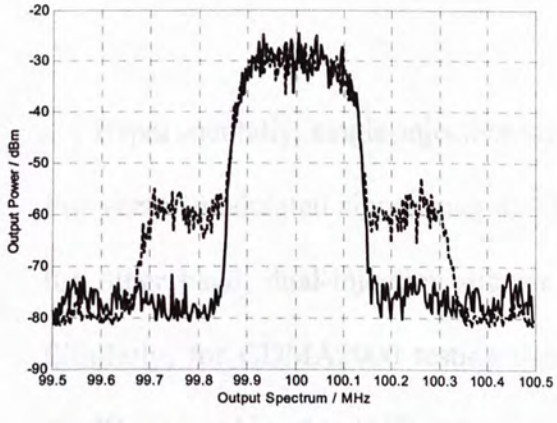

(a)

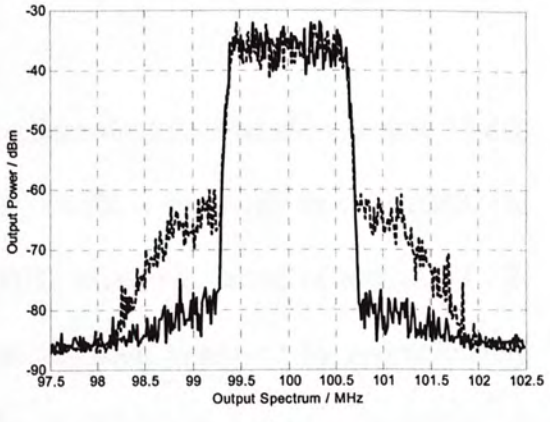

(b)

Figure 6.22 Vector-modulated signal test (a) PHS (b) CDMA2000

CHAPTER 7

CONCLUSIONS AND RECOMMENDATIONS FOR FUTURE WORK

7.1 CONCLUSIONS

In this thesis, the design and implementation of CMOS doubly balanced dual-gate mixer has been described. A mixer design example using 0.35 μm technology is presented. The mixer operates at an RF frequency of 900MHz with LO of 1GHz. The realized mixer exhibits a flat conversion gain over a wide frequency range and over 30 dB of port-to-port isolation. The mixer with buffer stages consumes a total current of 3.6 mA.

Generalized "low-frequency signal injection method" has been proposed to improve the linearity of doubly balanced dual-gate mixers. For simple implementation, single-injection scheme can be applied with only partial cancellation of IMD. For ultimate cancellation of IMD, dual-injection scheme is preferred.

Experimentally, single-injection scheme can reduce the IMD3 level by around 15 dB. For vector modulated signal such as CDMA2000, ACPR is improved by only 10dB. On the other hand, dual-injection scheme offers IMD3 reduction factor of almost 40 dB. Similarly, for CDMA2000 testing signal, ACPR has been improved by approximately 15 dB. The achievable IMD reduction factor of both schemes is basically limited by the presence of gain error in the baseband amplifiers. Moreover, the operating bandwidth of

the proposed method is mainly governed by the phase shift introduced by the low-frequency circuitry (memory effect). To summarize, the proposed linearization method has the following advantages:

- Simple circuitry.
- Suitable for monolithic integration.
- Minimal RF components.
- High IMD suppression ratio.

7.2 RECOMMENDATIONS FOR FUTURE WORK

Variation of environmental factor like temperature change may affect the operating conditions of the proposed method for optimum IMD suppression. For future work, the system may be improved by adding adaptive circuitry to compensate for such parameter shift.

Another major problem associated with RF transceiver design is generation of intermodulation distortion by the transmitter parts including power amplifier and up-conversion mixer. A potential application of the proposed techniques is to linearize the PA, up-conversion mixer and modulator altogether using a single circuitry implemented in CMOS technology.

APPENDIX

A1 CMOS TECHNOLOGY

MOSFET is the basic building block of very large-scale integrated (VLSI) circuits, which basically consists of both NMOS and PMOS devices. Nowadays, CMOS particularly sub-micron technology, plays an important role in digital, mixed-signal, as well as RF circuit design for wireless communication systems

A1.1 MOSFET structure

MOSFET is a four-terminal device (Illustrated in Figure A.1). The four terminals are: the silicon substrate (bulk)(B), the gate (G), the source (S), and the drain (D). When the bulk and the source are connected together, a voltage difference may appear between the bulk and the source to produce the "body effect". This effect may influence the normal operation of MOSFET.

Figure A.1 (a) illustrates a N-channel MOSFET (NMOS). NMOS uses P-type substrate and N^+ source and drain. Positive gate voltage is needed to create a surface channel of N-type carrier (electron) for conduction between the source and the drain. Similarly, PMOS using N-type substrate, P^+ source and drain. Electrical conduction is provided by P-type carrier (hole) which implies that a negative gate voltage is required for normal operation.

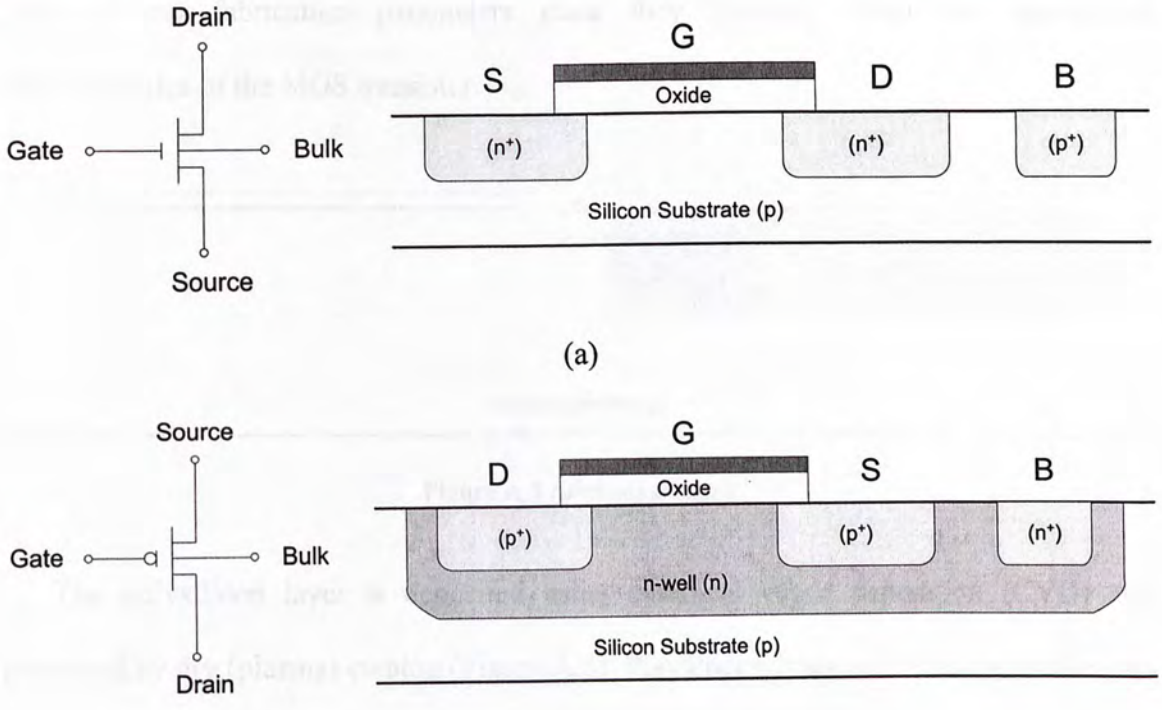

Figure A.1 Cross section view of MOSFET (a) NMOS (b) PMOS

A1.2 CMOS n-well process

Fabrication of CMOS integrated circuits is mostly based on n-well process [51]. Figures A.2-A.7 show the generalized fabrication sequence. It starts with a moderately doped p-type silicon substrate. Then, an initial oxide layer is grown on the entire surface. The n-well region is defined by the lithographic mask. Donor atoms (phosphorus) are implanted through this window in the oxide.

After the n-well region is formed, a thick field oxide is grown in the areas surrounding the transistors's active regions, and a thin gate oxide is grown on top of the active regions (Figure A.2). The thickness and quality of the gate oxide are two of the

most critical fabrication parameters since they strongly affect the operational characteristics of the MOS transistor.

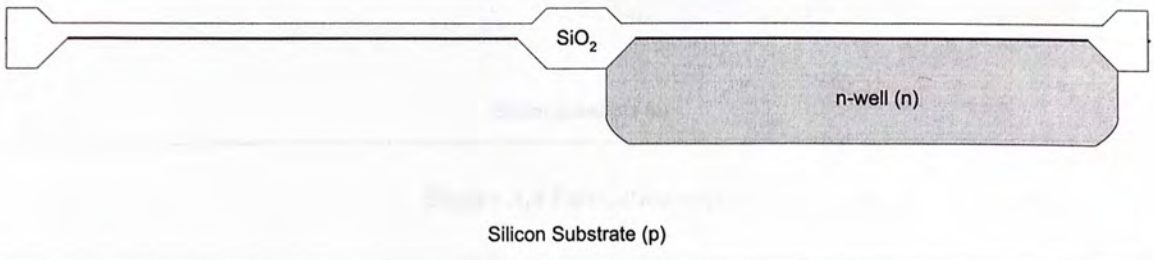

Figure A.2 Fabrication step 1

The polysilicon layer is deposited using chemical vapor deposition (CVD) and patterned by dry (plasma) etching (Figure A.3). Polysilicon lines will function as the gate electrodes of the NMOS and PMOS. Also, the polysilicon gates act as self-aligned masks for the source and drain implantations that follow this step.

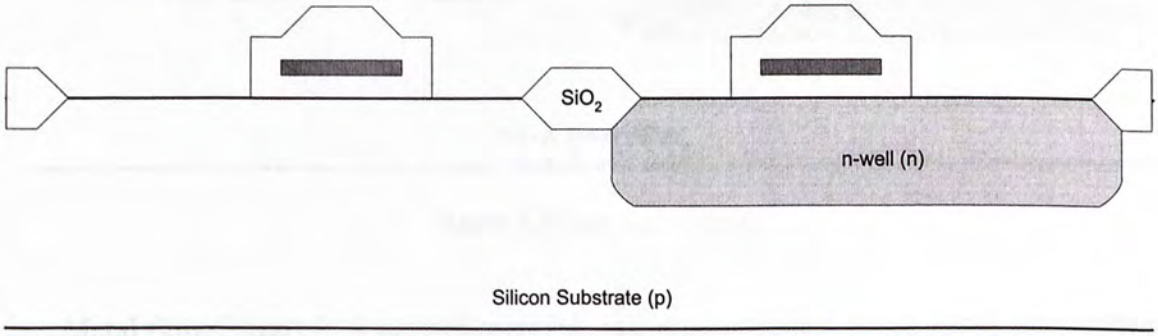

Figure A.3 Fabrication step 2

Using a set of two lithographic masks, n+ and p+ regions are implanted into the substrate and into the n-well, respectively. Also, the ohmic contacts to the substrate and to the n-well are implanted in this process step (Figure A.4).

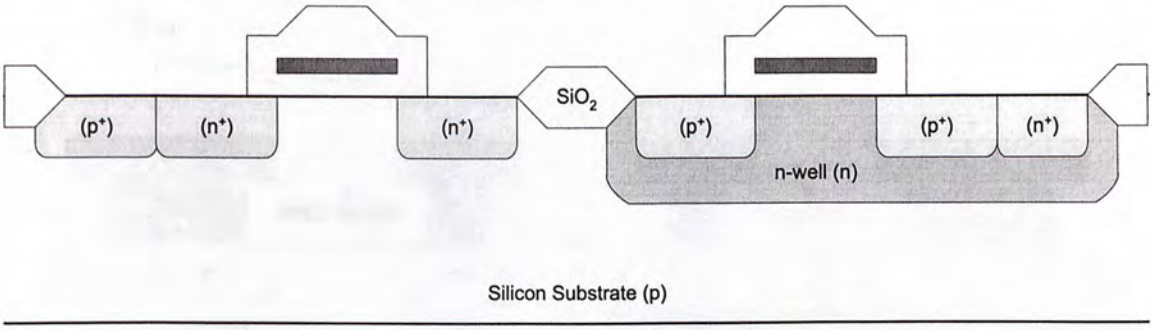

Figure A.4 Fabrication step 3

An insulating silicon dioxide layer is deposited over the entire wafer using CVD. Then, the contacts are defined and etched away to expose the silicon or polysilicon contact windows (Figure A.5). These contact windows are necessary to complete the circuit interconnections using the metal layer, which is formed in the next step.

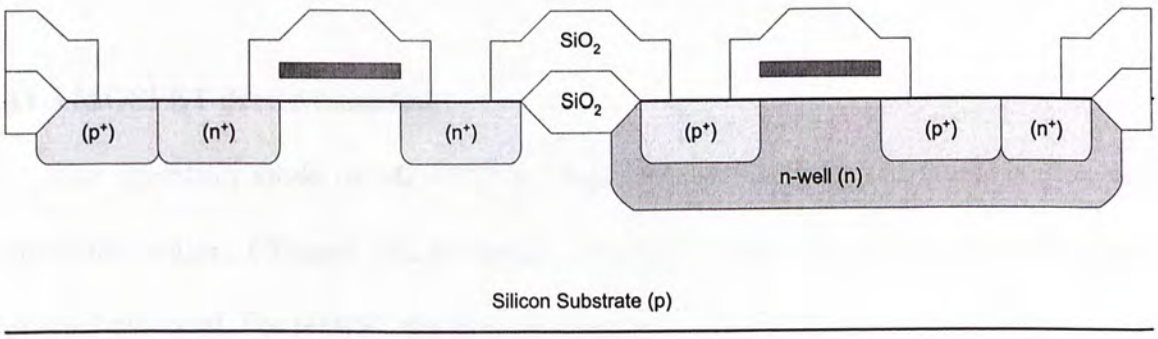

Figure A.5 Fabrication step 4

Metal (aluminum) is deposited over the entire chip surface using metal evaporation, and the metal lines are patterned through etching. Since the wafer surface is non-planar, the quality and the integrity of the metal lines created in this step are very critical and are ultimately essential for circuit reliability.

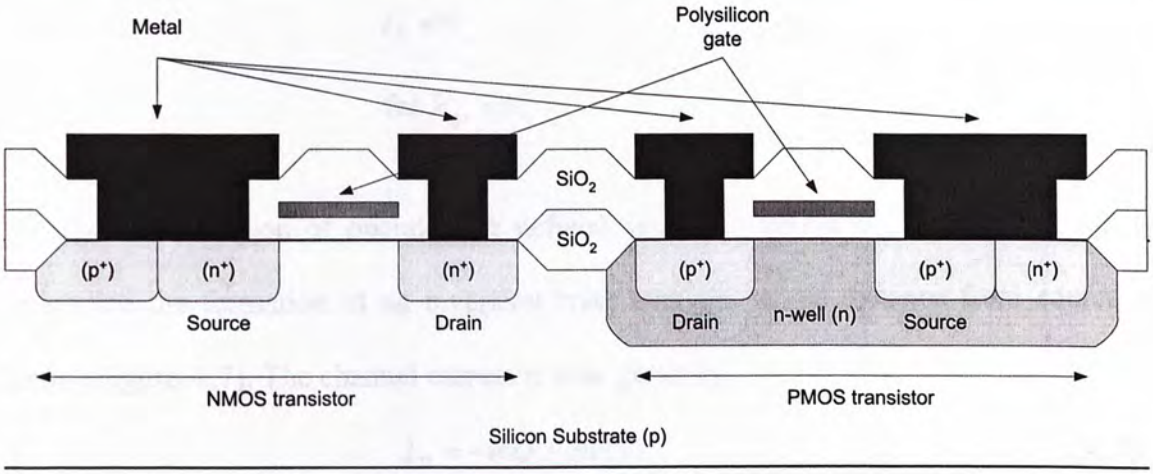

Figure A.6 Fabrication step 5

Figure A6 shows the cross-section view of one NMOS and PMOS transistor, the polysilicon gate and metal interconnections. The final step is to deposit the passivation layer (for protection) over the chip, except over wire-bonding pad areas.

A1.3 MOSFET device modeling

The operation mode of MOSFET is classified as: cutoff region, linear region and saturation region. Channel charge density depends on the gate oxide capacitance and channel potential. For NMOS, the channel charge density has the following form,

$$Q_n(y) = -C_{ox}\{[V_{gs} - V(y)] - V_t\} \tag{A.1}$$

where $Q_n(y)$ is the charge density at position y, C_{ox} is gate oxide capacitance per unit area and $V(y)$ is the channel potential at position y. When positive gate potential is not large enough for creating surface conduction channel ($Q_n(y) = 0$), the NMOS is in "OFF" state (cutoff). The channel current (I_D) can be written as:

$$I_D = 0$$
$$\text{for } V_{gs} < V_t \tag{A.2}$$

The linear region of operation is defined as one in which V_{gs} is large enough to guarantee the formation of an inversion layer over the whole distance from source to drain (Figure A.7). The channel current is now given by:

$$I_D = -WQ_n(y)v(y) \tag{A.3}$$

where W is the width of the device, $v(y)$ is electron velocity at positive y. For long-channel approximation, the electron velocity is simply the product of electron mobility (μ_n) and electric field (E), which gives,

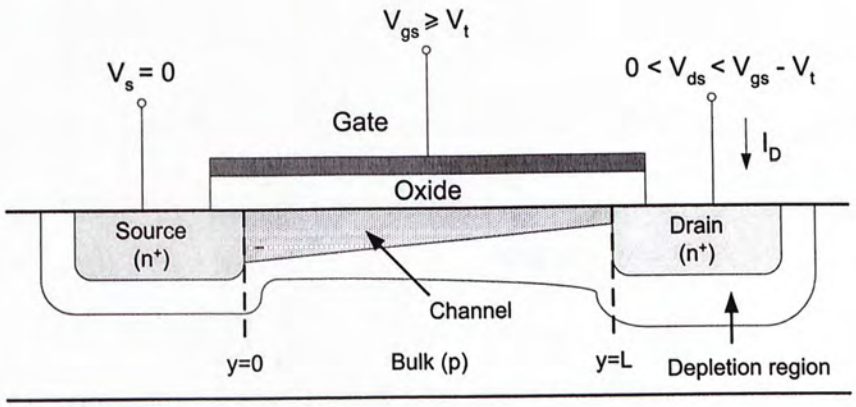

Figure A.7 Linear region operation of NMOS

$$I_D = -WC_{ox}\left[V_{gs} - V(y) - V_t\right]v(y)\mu_n E \tag{A.4}$$
$$= -WC_{ox}\left[V_{gs} - V(y) - V_t\right]v(y)\mu_n \frac{dV}{dy}$$

Subsequently, we have,

$$\int_0^L I_D dy = I_D L = \int_0^{V_{ds}} \mu_n W C_{ox} \left[V_{gs} - V(y) - V_t \right] v(y) dV \tag{A.5}$$

Solving the above equation, the channel current (linear region) is simply equal to,

$$I_D = \mu_n C_{ox} \frac{W}{L} \left[\left(V_{gs} - V_t \right) V_{ds} - \frac{V_{ds}^2}{2} \right] \tag{A.6}$$

$$\text{for } V_{gs} \geq V_t \text{ and } V_{ds} < V_{gs} - V_t$$

When V_{ds} is further increased until reaches certain value, the inversion layer will not extend all the way from source to drain. The channel is said to be "pinched-off" (Figure A.8). In this case, the MOSFET is in saturation region. The boundary between linear region and saturation region is defined by equation (A.7).

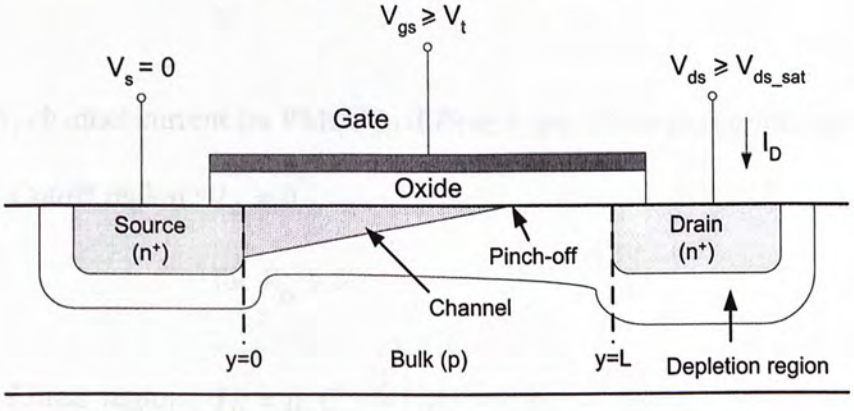

Figure A.8 Saturation region operation of NMOS

$$Q_n(L) = 0 \tag{A.7}$$

As a result, we have:

$$\left[V_{gs} - V_{ds} \right] - V_t = 0 \tag{A.8}$$

And, in saturation region, the current is defined as:

$$I_D = \frac{\mu_n C_{ox}}{2}\frac{W}{L}\left(V_{gs} - V_t\right)^2 \qquad \text{for } V_{gs} \geq V_t \text{ and } V_{ds} \geq V_{gs} - V_t \tag{A.9}$$

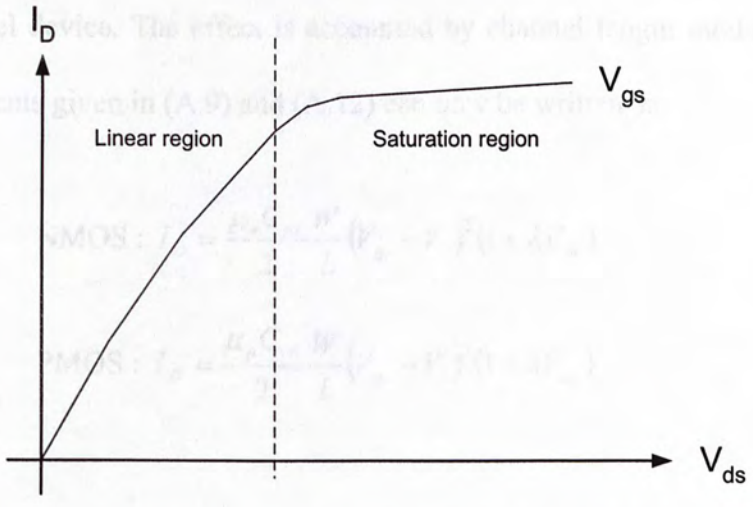

Figure A.9 Current voltage characteristics of NMOS

Similarly, channel current for PMOS in different operations are defined as follows:

$$\text{Cutoff region}: I_D = 0 \qquad \text{for } V_{gs} > V_t \tag{A.10}$$

$$\text{Linear region}: I_D = \mu_p C_{ox}\frac{W}{L}\left[\left(V_{gs} - V_t\right)V_{ds} - \frac{{V_{ds}}^2}{2}\right] \qquad \text{for } V_{gs} \leq V_t \text{ and } V_{ds} > V_{gs} - V_t \tag{A.11}$$

$$\text{Saturation region}: I_D = \frac{\mu_p C_{ox}}{2}\frac{W}{L}\left(V_{gs} - V_t\right)^2 \qquad \text{for } V_{gs} \leq V_t \text{ and } V_{ds} \leq V_{gs} - V_t \tag{A.12}$$

A1.4 Channel length modulation

When channel is pinch-off, the channel length becomes shorten. This effect can be ignored in long-channel device. However, the effective channel length become significant in short-channel device. The effect is accounted by channel length modulation (λ). The saturation currents given in (A.9) and (A.12) can now be written as:

$$\text{NMOS}: I_D = \frac{\mu_n C_{ox}}{2}\frac{W}{L}(V_{gs} - V_t)^2(1 + \lambda V_{ds}) \tag{A.13}$$

$$\text{PMOS}: I_D = \frac{\mu_p C_{ox}}{2}\frac{W}{L}(V_{gs} - V_t)^2(1 + \lambda V_{ds}) \tag{A.14}$$

A1.5 Body effect

There are some CMOS applications where the bulk and source terminals are at different protentials. For NMOS, when V_{bs} is positive, it opens a current path between the bulk and source. In the case of negative V_{bs}, the reverse bias of the bulk-to-source PN junction increases the threshold voltage of the NMOS (body effect). The threshold voltage V_t is now a function of V_{sb} and the channel current expressions have to be modified as follows:

$$\text{NMOS linear region}: I_D = \mu_n C_{ox}\frac{W}{L}\left[(V_{gs} - V_t(V_{sb}))V_{ds} - \frac{V_{ds}^2}{2}\right] \tag{A.15}$$

$$\text{NMOS saturation region}: I_D = \frac{\mu_n C_{ox}}{2}\frac{W}{L}(V_{gs} - V_t(V_{sb}))^2 \tag{A.16}$$

$$\text{PMOS linear region : } I_D = \mu_p C_{ox} \frac{W}{L}\left[\left(V_{gs} - V_t(V_{sb})\right)V_{ds} - \frac{V_{ds}^{\ 2}}{2}\right] \tag{A.17}$$

$$\text{PMOS saturation region : } I_D = \frac{\mu_p C_{ox}}{2}\frac{W}{L}\left(V_{gs} - V_t(V_{sb})\right)^2 \tag{A.18}$$

A2 MIXER'S NONLINEARITY ANALYSIS

In this section, the mixer is assumed to operate in weakly nonlinear region and in the presence of two-tone input signal. Due to the phase and amplitude imbalance of signals at the LO and RF inputs of the doubly balanced mixer, the mixing output can be expressed by,

$$V_M(t) = \frac{2}{\pi}\sum_{k=1}^{4}\left(g_{m1,k}v_{gs}(t) + g_{m2,k}v_{gs}^{\ 2}(t) + g_{m3,k}v_{gs}^{\ 3}(t)\right)R_L \times\left\{\cos(\omega_{LO}t) - \frac{1}{3}\cos(3\omega_{LO}t) + \frac{1}{5}\cos(5\omega_{LO}t) + \ldots.\right\} \tag{A.19}$$

$$\text{where } g_{m,k} = g_{m1,k} + g_{m2,k}v_{gs}(t) + g_{m3,k}v_{gs}^{\ 2}(t) \tag{A.20}$$

A2.1 First-order effect

The output signal produced by the first-order nonlinear coefficient is given by,

$$V_{M,1}(t) = \frac{2}{\pi}\sum_{k=1}^{4} g_{m1,k}v_{RF}R_L\left[\cos(\omega_{RF1}t) + \cos(\omega_{RF2}t)\right] \times\left\{\cos(\omega_{LO}t) - \frac{1}{3}\cos(3\omega_{LO}t) + \frac{1}{5}\cos(5\omega_{LO}t) + \ldots.\right\} \tag{A.21}$$

Consider the mixing operation produced by the LO fundamental frequency, the down-converted components (IF) is simple reduced to:

$$V_{M,1d}(t) = \frac{1}{\pi}\sum_{k=1}^{4} g_{m1,k} v_{RF} R_L \left[\cos((\omega_{LO} - \omega_{RF1})t) + \cos((\omega_{LO} - \omega_{RF2})t)\right]$$
$$= \frac{1}{\pi}\sum_{k=1}^{4} g_{m1,k} v_{RF} R_L \left[\cos((\omega_{IF} - \frac{\Delta\omega}{2})t) + \cos((\omega_{IF} + \frac{\Delta\omega}{2})t)\right] \quad \text{(A.22)}$$

A2.2 Second-order effect

The output signal produced by the second-order nonlinear coefficient is found as,

$$V_{M,2}(t) = \frac{2}{\pi}\sum_{k=1}^{4} g_{m2,k} {v_{RF}}^2 R_L \left[\cos(\omega_{RF1}t) + \cos(\omega_{RF2}t)\right]^2$$
$$\times\left\{\cos(\omega_{LO}t) - \frac{1}{3}\cos(3\omega_{LO}t) + \frac{1}{5}\cos(5\omega_{LO}t) + \ldots.\right\} \quad \text{(A.23)}$$

Consider the mixing operation produced by the LO fundamental frequency, the output components are therefore equal to:

$$V_{M,2d}(t) = \frac{1}{\pi}\sum_{k=1}^{4} g_{m2,k} {v_{RF}}^2 R_L \begin{bmatrix} \cos((\omega_{LO} - (\omega_{RF1} - \omega_{RF2}))t) \\ + \cos((\omega_{LO} - (\omega_{RF1} + \omega_{RF2}))t) \\ + \frac{1}{2}\cos((\omega_{LO} - 2\omega_{RF1})t) \\ + \frac{1}{2}\cos((\omega_{LO} - 2\omega_{RF2}t)) \end{bmatrix} \quad \text{(A.24)}$$

Clearly, these frequency components are far away from ω_{IF} and may be ignored in the analysis.

A2.3 Third-order effect

The output signal produced by the third-order nonlinear coefficient is given by,

$$V_{M,3}(t) = \frac{2}{\pi}\sum_{k=1}^{4} g_{m3,k} {v_{RF}}^3 R_L \left[\cos(\omega_{RF1}t) + \cos(\omega_{RF2}t)\right]^3 \times\left\{ \cos(\omega_{LO}t) - \frac{1}{3}\cos(3\omega_{LO}t) + \frac{1}{5}\cos(5\omega_{LO}t) + ... \right\} \tag{A.25}$$

Consider the mixing operation produced by the LO fundamental frequency, the output components can be expressed by:

$$V_{M,3d}(t) = \frac{1}{\pi}\sum_{k=1}^{4} g_{m3,k} {v_{RF}}^3 R_L \left[\begin{array}{l} \cos(\omega_{IF1}t) + \frac{1}{2}\cos(-\omega_{IF2}t) + \frac{1}{2}\cos((2\omega_{IF1} - \omega_{IF2})t) \\ + \frac{1}{2}\cos(\omega_{IF2}t) + \frac{1}{2}\cos((2\omega_{IF1} + \omega_{IF2})t) + \\ \frac{1}{4}\cos((2\omega_{IF2} + \omega_{IF1})t) + \frac{1}{4}\cos((2\omega_{IF2} - \omega_{IF1})t) \\ + \frac{1}{4}\cos(3\omega_{IF1}t) + \frac{1}{4}\cos(\omega_{IF1}t) + \end{array}\right]$$

$$+ \frac{1}{\pi}\sum_{k=1}^{4} g_{m3,k} {v_{RF}}^3 R_L \left[\begin{array}{l} \cos(\omega_{IF2}t) + \frac{1}{2}\cos(\omega_{IF1}t) + \frac{1}{2}\cos((\omega_{IF1} - 2\omega_{IF2})t) \\ + \frac{1}{2}\cos(\omega_{IF1}t) + \frac{1}{2}\cos((\omega_{IF1} + 2\omega_{IF2})t) + \\ + \frac{1}{4}\cos((2\omega_{IF1} - \omega_{IF2})t) + \frac{1}{4}\cos((2\omega_{IF1} - \omega_{IF2})t) \\ + \frac{1}{4}\cos(3\omega_{IF2}t) + \frac{1}{4}\cos(\omega_{IF2}t) \end{array}\right]$$

$$= \frac{1}{\pi}\sum_{k=1}^{4} g_{m3,k} {v_{RF}}^3 R_L \left[\begin{array}{l} \frac{9}{4}\cos(\omega_{IF1}t) + \frac{9}{4}\cos(\omega_{IF2}t) \\ + \frac{3}{4}\cos((2\omega_{IF1} - \omega_{IF2})t) + \frac{3}{4}\cos((2\omega_{IF2} - \omega_{IF1})t) \\ + \frac{3}{4}\cos((2\omega_{IF1} + \omega_{IF2})t) + \frac{3}{4}\cos((2\omega_{IF2} + \omega_{IF1})t) \\ + \frac{1}{4}\cos(3\omega_{IF1}t) + \frac{1}{4}\cos(3\omega_{IF2}t) \end{array}\right]$$

$$= \frac{1}{\pi}\sum_{k=1}^{4} g_{m3,k} v_{RF}{}^{3} R_L \begin{bmatrix} \frac{9}{4}\cos((\omega_{IF} - \frac{\Delta\omega}{2})t) + \frac{9}{4}\cos((\omega_{IF} + \frac{\Delta\omega}{2})t) \\ + \frac{3}{4}\cos((\omega_{IF} - \frac{3\Delta\omega}{2})t) + \frac{3}{4}\cos((\omega_{IF} + \frac{3\Delta\omega}{2})t) \\ + \frac{3}{4}\cos((2\omega_{IF1} + \omega_{IF2})t) + \frac{3}{4}\cos((2\omega_{IF2} + \omega_{IF1})t) \\ + \frac{1}{4}\cos(3\omega_{IF1}t) + \frac{1}{4}\cos(3\omega_{IF2}t) \end{bmatrix} \quad \text{(A.26)}$$

A2.4 Nonlinear IF spectrum

From equations (A.22) and (A.26), the frequency components appearing at the IF output are found as:

$$\begin{aligned} V_{IF}(t) &= \frac{1}{\pi}\sum_{k=1}^{4} g_{m1,k} v_{RF} R_L \left[\cos((\omega_{IF} - \frac{\Delta\omega}{2})t) + \cos((\omega_{IF} + \frac{\Delta\omega}{2})t)\right] \\ &\quad + \frac{1}{\pi}\sum_{k=1}^{4} g_{m3,k} v_{RF}{}^{3} R_L \begin{bmatrix} \frac{9}{4}\cos((\omega_{IF} - \frac{\Delta\omega}{2})t) + \frac{9}{4}\cos((\omega_{IF} + \frac{\Delta\omega}{2})t) \\ + \frac{3}{4}\cos((\omega_{IF} - \frac{3\Delta\omega}{2})t) + \frac{3}{4}\cos((\omega_{IF} + \frac{3\Delta\omega}{2})t) \end{bmatrix} \\ &\approx \frac{1}{\pi}\sum_{k=1}^{4} g_{m1,k} v_{RF} R_L \left[\cos((\omega_{IF} - \frac{\Delta\omega}{2})t) + \cos((\omega_{IF} + \frac{\Delta\omega}{2})t)\right] \\ &\quad + \frac{3}{4\pi}\sum_{k=1}^{4} g_{m3,k} v_{RF}{}^{3} R_L \left[\cos((\omega_{IF} - \frac{3\Delta\omega}{2})t) + \cos((\omega_{IF} + \frac{3\Delta\omega}{2})t)\right] \end{aligned} \quad \text{(A.27)}$$

A3 ARTIFICIAL IMD3 PRODUCED BY LOW-FREQUENCY SIGNAL INJECTION

Refer to the diagram shown in Figure 5.4, as the low-frequency signal is injected into the doubly balanced mixer via the drain circuitry, modulation of the device's transconductance occurs and it can be modeled as:

$$g_{m,k}(\text{mod\_a}) = g_{m,k}\left(1 + G_A\, v_{RF}{}^2 \cos(\Delta\omega t)\right) \tag{A.28}$$

where k = 1,2

$$g_{m,k}(\text{mod\_b}) = g_{m,k}\left(1 + G_B\, v_{RF}{}^2 \cos(\Delta\omega t)\right) \tag{A.29}$$

where k = 3,4

Subsequently, the output signal becomes:

$$\begin{aligned} V_M(t) = {} & \frac{1}{\pi}\sum_{k=1}^{2} g_{m,k}(\text{mod\_}a)R_L \times\left\{\cos(\omega_{LO}t) - \frac{1}{3}\cos(3\omega_{LO}t) + \frac{1}{5}\cos(5\omega_{LO}t) + \ldots.\right\} \\ & + \frac{1}{\pi}\sum_{k=3}^{4} g_{m,k}(\text{mod\_}b)R_L \times\left\{\cos(\omega_{LO}t) - \frac{1}{3}\cos(3\omega_{LO}t) + \frac{1}{5}\cos(5\omega_{LO}t) + \ldots.\right\} \\ = {} & \frac{1}{\pi}\sum_{k=1}^{4} g_{m,k}R_L \times\left\{\cos(\omega_{LO}t) - \frac{1}{3}\cos(3\omega_{LO}t) + \frac{1}{5}\cos(5\omega_{LO}t) + \ldots.\right\} \\ & + \frac{1}{\pi}\sum_{k=1}^{2} g_{m,k}(G_A v_{RF}{}^2 \cos\Delta\omega t)R_L \times\left\{\cos(\omega_{LO}t) - \frac{1}{3}\cos(3\omega_{LO}t) + \frac{1}{5}\cos(5\omega_{LO}t) + \ldots.\right\} \\ & + \frac{1}{\pi}\sum_{k=3}^{4} g_{m,k}(G_B v_{RF}{}^2 \cos\Delta\omega t)R_L \times\left\{\cos(\omega_{LO}t) - \frac{1}{3}\cos(3\omega_{LO}t) + \frac{1}{5}\cos(5\omega_{LO}t) + \ldots.\right\} \end{aligned} \tag{A.30}$$

Clearly, new signal components will be produced by the injected low-frequency signals. Consider the mixing operation associates with the first-order nonlinearity coefficient, the new down-converted signal $V_{M\_i,1d}(t)$ is simply given by:

$$
\begin{aligned}
V_{M\_i,1d}(t) &= \frac{1}{\pi}\sum_{k=1}^{2} g_{m1,k} G_A v_{RF}{}^3 R_L \left[\cos((\omega_{IF}-\frac{\Delta\omega}{2})t)+\cos((\omega_{IF}+\frac{\Delta\omega}{2})t)\right]\cos(\Delta\omega t) \\
&+ \frac{1}{\pi}\sum_{k=3}^{4} g_{m1,k} G_B v_{RF}{}^3 R_L \left[\cos((\omega_{IF}-\frac{\Delta\omega}{2})t)+\cos((\omega_{IF}+\frac{\Delta\omega}{2})t)\right]\cos(\Delta\omega t) \\
&= \frac{1}{2\pi}\sum_{k=1}^{2} g_{m1,k} G_A v_{RF}{}^3 R_L \begin{bmatrix} \cos((\omega_{IF}-\frac{3\Delta\omega}{2})t)+\cos((\omega_{IF}-\frac{\Delta\omega}{2})t) \\ +\cos((\omega_{IF}+\frac{\Delta\omega}{2})t)+\cos((\omega_{IF}+\frac{3\Delta\omega}{2})t) \end{bmatrix} \\
&+ \frac{1}{2\pi}\sum_{k=3}^{4} g_{m1,k} G_B v_{RF}{}^3 R_L \begin{bmatrix} \cos((\omega_{IF}-\frac{3\Delta\omega}{2})t)+\cos((\omega_{IF}-\frac{\Delta\omega}{2})t) \\ +\cos((\omega_{IF}+\frac{\Delta\omega}{2})t)+\cos((\omega_{IF}+\frac{3\Delta\omega}{2})t) \end{bmatrix} \\
&= \frac{1}{2\pi}\sum_{k=1}^{2} g_{m1,k} G_A v_{RF}{}^3 R_L \left[\cos((\omega_{IF}-\frac{\Delta\omega}{2})t)+\cos((\omega_{IF}+\frac{\Delta\omega}{2})t)\right] \\
&+ \frac{1}{2\pi}\sum_{k=3}^{4} g_{m1,k} G_B v_{RF}{}^3 R_L \left[\cos((\omega_{IF}-\frac{\Delta\omega}{2})t)+\cos((\omega_{IF}+\frac{\Delta\omega}{2})t)\right] \\
&+ \frac{1}{2\pi}\sum_{k=1}^{2} g_{m1,k} G_A v_{RF}{}^3 R_L \left[\cos((\omega_{IF}-\frac{3\Delta\omega}{2})t)+\cos((\omega_{IF}+\frac{3\Delta\omega}{2})t)\right] \\
&+ \frac{1}{2\pi}\sum_{k=3}^{4} g_{m1,k} G_B v_{RF}{}^3 R_L \left[\cos((\omega_{IF}-\frac{3\Delta\omega}{2})t)+\cos((\omega_{IF}+\frac{3\Delta\omega}{2})t)\right]
\end{aligned}
\tag{A.31}
$$

As a result, artificial IMD3 is produced at the IF output which may be shown as:

$$
\begin{aligned}
V_{A\_IMD3}(t) &= \frac{1}{2\pi}\sum_{k=1}^{2} g_{m1,k} G_A v_{RF}{}^3 R_L \left[\cos((\omega_{IF}-\frac{3\Delta\omega}{2})t)+\cos((\omega_{IF}+\frac{3\Delta\omega}{2})t)\right] \\
&+ \frac{1}{2\pi}\sum_{k=3}^{4} g_{m1,k} G_B v_{RF}{}^3 R_L \left[\cos((\omega_{IF}-\frac{3\Delta\omega}{2})t)+\cos((\omega_{IF}+\frac{3\Delta\omega}{2})t)\right]
\end{aligned}
\tag{A.32}
$$

AUTHOR'S PUBLICATION LIST

[1] C. F. Au-Yeung and K. K. M Cheng, "CMOS Mixer Linearization by the Low-Frequency Signal Injection Method", IEEE MTT-S International Microwave Symposium, Philadelphia, June 2003.

[2] C. F. Au-Yeung and K. K. M Cheng, "Realization of Fully Integrated CMOS Double-Balanced Mixer with On-Chip Active Baluns", to be presented, Asia-Pacific Microwave Conference, Seoul, Nov 2003.

[3] K. K. M Cheng and C. F. Au-Yeung, "Application of Generalized Low-Frequency Signal Injection Method to the Linearization of CMOS Mixers", submitted to IEEE IEEE Transactions on Microwave Theory and Techniques.

REFERENCES

[1] S. A. Maas, "Microwave Mixer", Artech House, Inc., 1991.

[2] T. H. Lee "The Design of CMOS Radio-Frequency Integrated Circuits", Cambridge University Press, 1998.

[3] B. Razavi, "RF Microelectronics", Prentice Hall, 1998.

[4] B. Rezavi, "A 1.5 V 900 MHz downconversion mixer," IEEE International Solid-State Circuits Conference, pp. 48 –49, Feb 1996.

[5] H. K. Chiou and H. H. Lin "A miniature MMIC double doubly balanced mixer using lumped dual balun for high dynamoc receiver application", IEEE Microwave and Guided Wave Letters, vol. 7, no. 8, Aug 1997.

[6] K. L. Fong, C. D. Hull and R. G. Meyer " A class AB monolithic mixer for 900 MHz applications", IEEE Journal of Solid-State Circuits, vol. 32, no. 8, pp. 1166-1172, Aug 1997.

[7] K. L. Fong and R. G. Meyer "Monolithic RF active mixer design", IEEE Transactions on Circuits and Systems – II : Analog and Digital Signal Processing, vol. 46, no. 3, pp. 231-239, Mar 1999.

[8] S. Colomines, T. Arnaud, R. Plana, T. Parra and J. Graffeuil, "Design of high performances Gilbert-cell mixers for GSM/DCS front-ends", IEEE Radio Frequency Integrated Circuits Symposium, pp. 143-146, Jun 1998.

[9] J. R. Long, "A low-voltage 5.1-5.8GHz image-reject downconverter RF IC", IEEE Journal of Solid-State Circuits, vol. 35, no. 9, pp. 1320-1328, Sep 2000.

[10] J. W. M. Rogers, J. A. Macedo and C. Plett, "A completely integrated 1.9 GHz receiver front-end woth monolithic image-reject filter and VCO", IEEE Transactions on Microwave Theory and Techniques, vol. 50, no. 1, pp. 210-215, Jan 2002.

[11] B. Kim, K. S. Nah, T. W. Ahn, H. I. Lee, J. K. Cho and B. H. Park, "A 2.6V GSM/PCN dual band variable gain low noise RF down conversion mixer", IEEE Radio Frequency Integrated Circuits Symposium, pp. 134-140, Jun 2002.

[12] J. Crols and M. S. J. Steyaert, "A 1.5 GHz highly linear CMOS downconversion mixer," IEEE Journal of Solid-State Circuits, vol. 30, no. 7, pp. 736 – 742, Jul 1995.

[13] J. Crols and M. S. J. Steyaert, "A single-chip 900 MHz CMOS receiver front-end with a high performance low-IF topology," IEEE Journal of Solid-State Circuits, vol. 30, no. 12, Dec 1995.

[14] A. Rofougaran, J. Y. C. Chang, M. Rofougaran and A. A. Abidi, "A 1 GHz CMOS RF front-end IC for a direct-conversion wireless receiver," IEEE Journal of Solid-State Circuits, vol. 31, no. 7, pp. 880 – 889, Jul 1996.

[15] A. N. Karanicolas, "A 2.7-V 900-MHz CMOS LNA and mixer", IEEE Journal of Solid-State Circuits, vol. 31, no. 12, pp. 1939-1994, Dec 1996.

[16] P. R. Kinget and M. S. J. Steyaert, "A 1-GHz CMOS up-conversion mixer," IEEE Journal of Solid-State Circuits, vol. 32, no. 12, pp. 370 – 376, Mar 1997.

[17] P. J. Sullivan, B. A. Xavier and W. H. Ku, "Low voltage performance of a microwave CMOS Gilbert cell mixer", IEEE Journal of Solid-State Circuits, vol. 32, no. 7, pp. 1151-1155, Jul 1997.

[18] P. J. Sullivan, B. A. Xavier and W. H. Ku, "A common source input cross coupled quad CMOS mixer", Proceedings of the 40th Midwest Symposium on Circuits and Systems, pp. 152-151, Aug 1997.

[19] G. Kathiresan and C. Toumazou, "A low voltage bulk driven downconversion mixer core", IEEE International Symposium on ISCAS , vol 2, pp. 598-901, Jun 1999.

[20] P. J. Sullivan, B. A. Xavier and W. H. Ku, "Doubly balanced dual-gate CMOS mixer", IEEE Journal of Solid-State Circuits, vol. 34, no. 6, pp. 878-881, Jun 1999.

[21] P. B. Khannur and K. S. Ling, "A 2.45 GHz fully-differential CMOS image-reject mixer for bluetooth application", IEEE MTT-S International Microwave Symposium, vol. 1, pp. 549-552, Jun 2002.

[22] W. Sheng, B. Xia, A. Emira, C. Xin, A. Y. Valero-Lopez, S. T. Moon and E. Sánchez-Sinencio, "A 3V, 0.35μm CMOS Bluetooth receiver IC", IEEE Radio Frequency Integrated Circuits Symposium, pp. 107-110, Jun 2002.

[23] F. Beffa, R. Vogt, W. Bächtold, E. Zellweger and U. Lott, "A 6.5-mW receiver front-end for Bluetooth in 0.18-μm CMOS", IEEE MTT-S International Microwave Symposium", vol. 1, pp. 501-504, Jun 2002.

[24] B. Gilbert, "A precise four quadrant multiplier with subnanosecond response", IEEE Journal of Solid-State Circuits, vol. 3, no. 4, pp. 365–373, Dec 1968.

[25] B. Razavi, "Design of Analog CMOS Integrated Circuits", McGraw Hill, 2001.

[26] S. M. Kang and Y. Leblebigi, "CMOS Digital Integrated Circuits – Analysis and Design", WCB/McGraw Hill, 1999.

[27] A. Hastings, "The Art of Analog Layout", Prentice Hall, 2001.

[28] Y. Kinoshita, K. Sekine, A. Dooi and A. Iso, "Linearization of harmonic controlled high efficiency power amplifier", IEEE Vehicular Technology Conference, pp. 445-450. May1991.

[29] M. R. Moazzam and C. S. Aitchison "A low third order intermodulation amplifier with harmonic feedback circuitry", IEEE MTT-S International Microwave Symposium, vol. 2, pp. 827-830, Jun 1996.

[30] A. N. D'Andrea, V. Lottici and R. Reggiannini, "RF power amplifier linearization through amplitude and phase predistortion", IEEE Transactions on Communications, vol. 44, no. 11, pp. 1477-1484, Nov 1996.

[31] S. G. Kang, I. K. Lee and L. S. Yoo, "Analysis and design of feedforward power amplifier", IEEE MTT-S International Microwave Symposium, vol. 3, pp. 1519 – 1522, Jun 1997.

[32] W. Struble, F. McFrath, I. Harrington and P. Nagle "Understanding linearity in wireless communication amplifiers", IEEE Journal of Solid-State circuits, vol. 32, no. 9, pp 1310-1318, Sep 1997.

[33] M. Faulkner, "Amplifier Linearization Using RF Feedback and Feedforward Techniques", IEEE Transactions on Vehicular Technology, vol. 47, no. 1, Feb 1998.

[34] R. Nagy, J, Bartolic and B. Modlic, "GaAs MESFET small signal amplifier intermodulation distortion improvement by the second harmonic termination", IEEE Electrotechnical Conference, vol. 1, pp 358-361, May 1998.

[35] Y. Kim, Y. Yang, S. Kang and B. Kim, "Linearization of 1.85 GHz amplifier using feedback predistortion loop", IEEE MTT-S International Microwave Symposium, vol. 3, pp. 1675-1678, Jun 1998.

[36] D. Jing, W.S. Chan, S. M. Li and C. W. Li, "New linearization method using interstage second harmonic enhancement", IEEE Microwave and Guided Wave Letters, vol. 8, no. 11, Nov 1998.

[37] D. Jing, S. M. Li, C. S. Yu and W. S. Chan, "A new linearization method for reducing adjacent channel power in PHS amplifiers", IEEE Asia-Pacific Microwave Conference, pp. 1427-1430, Dec 1998.

[38] C. S. Yu, W. S. Chan and W. L. Chan "1.9 GHz low loss varactor diode pre-distorter", IEEE Electronics Letters, vol. 35, no. 20, pp. 1681-1682, Sep 1999.

[39] Y. Yang and B. Kim "A new linear amplifier using low-frequency second-order intermodulation component feedforwarding", IEEE Microwave and Guided Wave Letters, vol. 9, no. 10, pp. 419-421, Oct 1999.

[40] J. Yi, Y. Yang, M. Park, W. Kang and B. Kim, "Analog predistortion linearizer for high-power RF amplifier", IEEE Transactions on Microwave Theory and Techniques, vol. 48, no. 12, pp. 2709-2713, Dec 2000.

[41] C. W. Fan and K. K. M. Cheng, "Theoretical and experimental study of amplifier linearization based on harmonic and baseband signal injection technique", IEEE Transactions on Microwave Theory and Techniques, vol. 50, no. 7, Jul 2002.

[42] C. S. Leung, and K. K. M Cheng, "A new approach to amplifier linearization by the generalized baseband signal injection method" IEEE Microwave and Wireless Components Letters, vol. 12, no. 9, pp. 336-338, Sep 2002.

[43] K. K. M Cheng, and C. S. Leung, "A novel generalized low-frequency signal-injection method for multistage amplifier linearization", IEEE Transactions on Microwave Theory and Techniques, vol. 51, no. 2, pp. 553-559, Feb 2003.

[44] J. H. K. Vuolevi, T. Rahkonen, and J. P. A. Manninen, "Measurement technique for characterizing memory effects in RF power amplifiers" IEEE Trans. Microwave Theory and Techniques, vol. 49, no. 8, pp. 1383-1389, Aug 2001.

[45] N. B. D. Carvalho, and J. C. Pedro, "A comprehensive explanation of distortion sideband asymmetries" IEEE Transactions on Microwave Theory and Techniques, vol. 50, no. 9, pp. 2090-2101, Sep 2002.

[46] K. L. Fong and R. G. Meyer, "High-frequency nonlinearity analysis of common-emitter and differential-pair transconductance stages", IEEE Journal of Solid-State Circuits, vol. 33, no. 4, pp. 548-555, Apr 1998.

[47] Thomas J. Ellis, "A modified feed-forward technique for mixer linearization", Microwave Symposium Digest, IEEE MTT-S International Microwave Symposium, vol. 3, pp. 1423 –1426, Jun 1998.

[48] M. Chongcheawchamnan and I. D. Robertson, "Linearised microwave mixer using simplified feedfoward technique", IEEE Electronics Letters, vol. 35, no. 9 , pp. 724 – 725, Apr 1999.

[49] Youngwook Kim, Youngsik Kim and S. Lee, "Linearized mixer using predistortion technique", IEEE Microwave and Wireless Components Letters, vol. 12, no. 6, Jun 2002.

[50] M. Chongcheawchamnan, C. Y. Ng, and I. D. Robertson, "Difference frequency injection linearisation technique for mixer systems", IEEE Electronics Letters, vol. 38, no. 23, pp. 1450-1452, Nov 2002.

[51] S. A. Mass, "Nonlinear Microwave Circuit", Artech House, Inc., 1988.